This is the peer-reviewed, final accepted version for American Mineralogist, published by the Mineralogical Society of America.
The published version is subject to change. Cite as Authors (Year) Title. American Mineralogist, in press.
DOI: https://doi.org/10.2138/am-2022-8241. http://www.minsocam.org/

Revision 2

Titanite geochemistry and textures: implications for magmatic and post-magmatic processes in the Notch Peak and Little Cottonwood granitic intrusions, Utah

AUTHOR LIST

Porter K. Henze[1], Eric H Christiansen[1], Bart J. Kowallis[1], Michael J. Dorais[1], Haley D. Mosher[1], Lauren M. Franzen[1], Alec J. Martin[1], and Peter I. Nabelek[2]

1. Department of Geological Sciences, Brigham Young University, Provo, UT 84602
2. Department of Geological Sciences, University of Missouri, Columbia MO 65211

This is the peer-reviewed, final accepted version for American Mineralogist, published by the Mineralogical Society of America.
The published version is subject to change. Cite as Authors (Year) Title. American Mineralogist, in press.
DOI: https://doi.org/10.2138/am-2022-8241. http://www.minsocam.org/

ABSTRACT

Textural and compositional variations in titanite constrain the roles of magma mixing and hydrothermal alteration in two plutons in central Utah: the Jurassic Notch Peak and the Oligocene Little Cottonwood stocks. In the Notch Peak intrusion, magmatic titanite grains usually have oscillatory zones combined with BSE-bright sector zones, in some cases surrounding simple unzoned cores. These grains are frequently overprinted by hydrothermal titanite with low concentrations of high field strength elements (HFSE). Magmatic titanite has an average $\delta^{18}O$ of 6.0‰ and post-magmatic titanite is 6.2‰, as analyzed by SIMS. Average Zr-in-titanite temperatures are also similar with 718°C for magmatic and 711°C for hydrothermal titanite. These observations indicate simple magmatic growth, followed by hydrothermal alteration by magmatic fluids. Titanite in aplite dikes and sills has lower concentrations of all trace elements except F. Many titanite grains in the aplites have late overgrowths of high-Fe titanite. This high-Fe titanite has $\delta^{18}O$ of 6‰ and average Zr-in-titanite temperature of 718°C and likely precipitated from a last flush of exsolved magmatic water enriched in Cl and Fe.

Titanite in the Little Cottonwood stock typically has distinct patchy cores with rounded and embayed ilmenite inclusions. Mafic enclaves have abundant titanite that is similar in texture and $\delta^{18}O$ (5.1‰) to titanite in the host ($\delta^{18}O$ = 4.9‰), but it has a slightly higher average Zr-in-titanite temperature (731° versus 717°C). The patchy cores in the enclaves have the highest average Zr-in-titanite temperature (759°C) and distinctive REE patterns. The textural and compositional data indicate that a hotter, more reduced, ilmenite-bearing mafic magma mixed into an oxidized felsic magma, destabilizing existing ilmenite and allowing crystallization of titanite. In the granodiorite and in the enclaves, hydrothermal growth of titanite is evidenced by distinct narrow rims as well as anhedral titanite that grew between sheets of chloritized biotite.

Secondary hydrothermal titanite typically has lower concentrations of most HFSE, but is relatively enriched in F, Mg, Mo, and U, and it has higher Nb/Ta and lower Th/U ratios. Post-magmatic titanite also has strikingly different REE patterns than magmatic titanite, including the absence of pronounced Eu anomalies and lower REE abundances. These chemical features are controlled by element solubilities in aqueous fluids. In most cases, hydrothermal titanite has $\delta^{18}O$ values similar to magmatic titanite, indicating alteration and recrystallization from exsolved magmatic fluids. The involvement of meteoric water with low $\delta^{18}O$ is evident locally; individual spots have $\delta^{18}O$ as low as 1.7‰ in the Little Cottonwood stock.

Titanite compositions and textures provide important insights into the origins of granitic rocks and can be used to distinguish separate batches of magma, gauge the evolution of magmatic rocks, assess mixing processes, and infer compositions of mixing components. Because titanite also forms hydrothermally, it retains hints about the composition, temperature, and oxygen fugacity of the hydrothermal fluids and reveals details about titanite-forming reactions. However, the Al-in-titanite geobarometer does not yield realistic pressures of crystallization and the use of titanite as a geochronometer is compromised by the development of U-rich hydrothermal titanite.

Keywords: Titanite, Notch Peak granite, Little Cottonwood stock, granite, mafic enclave, $\delta^{18}O$, magma mixing, hydrothermal alteration

INTRODUCTION

The compositions and textures of accessory minerals are powerful tools for interpreting pluton construction and evolution and have been the focus of numerous petrological studies. For example, titanite incorporates U, rare earth elements (REE), and high field strength elements (HFSE), that provide clues to crystallization ages and environments, changes in magma composition, and post-magmatic histories (e.g., McLeod et al. 2011; Jiang et al. 2016; Laurent et al. 2017; Rossetti et al. 2017; Pan et al. 2018; Bruand et al. 2019). Titanite is common in plutonic, volcanic, and metamorphic rocks and has several petrogenetic advantages over zircon, a commonly studied accessory phase. For example, the presence or absence of titanite may indicate relative oxygen fugacity, as titanite is stable under high oxygen fugacity, but unstable at low oxygen fugacity, where ilmenite crystallizes instead (Wones 1989; Xirouchakis et al. 2001; Angiboust and Harlov 2017; Kohn 2017). Like zircon, titanite has low elemental diffusion rates so magmatic zonation is typically preserved (Paterson et al. 1989; Cherniak 2010; Kohn 2017); titanite can endure greenschist facies metamorphic conditions for millions of years before 1% of the grain will exchange oxygen with its surroundings (King et al. 2001). Titanite ($CaTiSiO_5$) compositions range more widely than zircon with three cation sites: a tetrahedral site with Si may have minor amounts of Al, an octahedral site with Ti accommodates highly charged elements such as Al, Zr, Fe^{3+}, Nb, and Ta, and a 7-fold decahedral site with Ca that incorporates Na, Sr, REE, Y, U, and Pb (Speer and Gibbs 1976; Deer et al. 1982; Frost et al. 2001b; Kohn 2017). Titanite also has an underbonded O site into which OH^- and F^- may substitute. These substitutions make it a good tracer of diverse geologic processes at high (~800°C) and low temperatures (~600°C) in the presence of melt or hydrothermal fluids. Moreover, in contrast to zircon, titanite is much more commonly affected by post-magmatic dissolution and

recrystallization in hydrothermal fluids. While titanite can incorporate hundreds of ppm of U, which is vital for geochronological studies, it also incorporates significant common Pb, making U-Pb dates harder to interpret than for zircon (Frost et al.2001b; Aleinikoff et al. 2002; Kohn 2017). Titanite has also been used as a geothermobarometer (Hayden et al. 2008; Erdman et al. 2019). In short, elemental variations and ages reflect a wide range of processes, including magmatic growth, subsequent cooling, secondary fluid alteration, and deformation (McLeod et al. 2011; Bonamici et al. 2015; Garber et al. 2017).

In this paper, we present a textural and geochemical study of titanite in two granitic intrusions—the Notch Peak pluton and the Little Cottonwood stock. We use titanite textures, geothermometry, $\delta^{18}O$, and major and trace element compositions to answer these questions:

1. Did titanite form by magmatic or post-magmatic processes? What are the textural, elemental, and isotopic characteristics of each type?
2. What was the nature of the fluid that caused secondary alteration of the plutons?
3. What was the role of magma mixing in the origin of titanite in these plutons?

GEOLOGIC SETTING OF THE INTRUSIONS

The Jurassic Notch Peak pluton is exposed in the House Range of west-central Utah and the Oligocene Little Cottonwood stock lies in the Wasatch Mountains (Fig. 1). These granitic intrusions formed during Mesozoic and middle Cenozoic subduction (Christiansen et al. 2015; Yonkee and Weil, 2015; Best et al. 2016). Erosion accompanying late Cenozoic extension exposed the intrusions (Nabelek et al. 1986; John 1989; Hintze and Kowallis 2021).

Notch Peak pluton

The Notch Peak granite (*sensu stricto*) intruded into interbedded Paleozoic limestone and argillites during the Jurassic period about 169 ± 3 Ma at a depth of 4-5 km (Gehman 1958; Lee et al. 1986; Nabelek and Labotka 1993; Hintze and Davis 2002; Supplement Figs. A1 to A3). The pluton has an area of about 18 km^2 and is made up of three sequentially intruded units (Nabelek

et al. 1986). The earliest is granite found along the borders of the pluton, especially along the northeastern corner (Fig 1). This granite was subsequently intruded by "Quartz Monzonite I" (QMI) while the granite was at least partially solidified, and then by "Quartz Monzonite II" (QMII) in the eastern part of the pluton (Fig. 1). All three units are texturally and mineralogically similar, but silica increases from QMI, to QMII, to granite. The granite unit tends to have the most variable texture ranging from porphyritic to seriate. The quartz monzonites are coarser-grained and seriate. However, all units are granite according to the IUGS modal and chemical classification schemes (Fig. 2) and, for simplicity, we refer to the pluton as the Notch Peak granite. Abundant 1-6 m thick aplite dikes and sills formed along the southern and western border and cut both the intrusion and the surrounding sedimentary rock.

Major minerals are similar in all three units and include plagioclase, K-feldspar, quartz, and biotite; hornblende is only in a few samples. Accessory minerals such as titanite, apatite, zircon, ilmenite, allanite, and magnetite are in all phases, including the aplites. Based largely on O-isotopic data, Nabelek et al. (1983) and Novick and Labotka (1990) concluded that late hydrothermal fluids of magmatic origin slightly altered the pluton and formed an extensive contact aureole in the carbonate wall rocks.

Little Cottonwood stock

The Little Cottonwood stock, 32 km south of Salt Lake City, is part of the Wasatch Igneous Belt, an east-west trend of at least eleven Paleogene intrusions and an associated volcanic field in central Utah. At about 30 Ma, the Little Cottonwood magmas intruded a deformed succession of Proterozoic metamorphic rocks, Neoproterozoic quartzite, and Paleozoic miogeoclinal sedimentary rocks (Hanson 1995; Vogel et al. 2001; Smyk et al. 2018; McKean

and Solomon 2018; Jensen et al. 2022). Later, movement on the Wasatch normal fault produced flexural-isostatic uplift and tilted the range to the east. Current exposures of the stock came from paleodepths of 11 to 5.6 km (Parry and Bruhn 1987; John 1989; Kowallis et al. 1990; Ehlers et al. 2003). The stock has an area of 115 km^2 (Hanson 1995), about six times larger than the Notch Peak intrusion (Fig. 1 & Supplement Fig. A4).

The northern and eastern parts of the Little Cottonwood stock are compositionally and texturally zoned from a finer-grained, less-silicic outer zone to a coarser-grained, more-silicic zone in the center (Marsh and Smith 1997). It consists of granite and granodiorite with some quartz monzonite (Hanson 1995; Fig. 2). We refer to the main mass as granodiorite to contrast it with the Notch Peak granite. Major minerals are plagioclase, K-feldspar, quartz, biotite, and hornblende, while accessory minerals include titanite, apatite, zircon, magnetite, and ilmenite (Hanson 1995; Henze 2020). Near the Wasatch fault to the west, the granodiorite is commonly sheared and deformed, but still similar in composition to the unsheared granodiorite. The Little Cottonwood intrusion contains numerous mafic enclaves and schlieren interspersed throughout much of the stock (Hanson 1995; Marsh and Smith 1997; Supplement Fig. A5). Locally, the intrusion is hydrothermally altered with weak Mo mineralization. John (1989) suggested that the fluids were magmatically derived, based on unpublished O and H isotopic data.

METHODS AND RESULTS

Titanite-bearing rocks were collected from both intrusions (Fig. 1). Whole-rock samples were analyzed for major and trace element compositions by X-ray fluorescence (XRF) spectrometry at Brigham Young University (BYU) using techniques outlined in Dailey et al. (2018). Subsets of Notch Peak and Little Cottonwood samples were also analyzed commercially

(ALS Global in Reno, Nevada) by ICP-MS for additional trace elements including REEs. The results are presented in Fig. 2 and in Supplement C1.

Thin sections were studied using backscatter electron (BSE) imagery on a Helios Nanolab 600 FEI with an Elstar in-lens BSE detector and later with an Apreo Scanning Electron Microscope at BYU. BSE systems were operated at 15.0 kV, 6.4 nA, and a working distance of around 10 mm. The BSE images are shown below and in Supplement A. The textural classification developed using these images is described in Table 1.

Individual grains of titanite were analyzed by electron microprobe for Si, Al, Ti, Mg, Fe, Ca, Na, Mn, Nb, Y, La, Ce, Nd, Sm, and F using a Cameca SX-50 with a 1 μm beam diameter at 15 kV and a 30 nA at BYU. Titanite formulas were recalculated assuming a total of 16 cations per formula unit (pfu). Tables 2 and 4 list average compositions and the full data set is in Supplement C2. Repeat analyses of the Taylor sphene, used as a reference, are given in Supplement C3.

Oxygen isotope analysis of titanite was performed at the University of Wisconsin-Madison WiscSIMS lab on a Cameca IMS-1280 ion microprobe. 1-inch round sample mounts were prepared from polished thin sections. Sections were polished to achieve <1 μm of surface relief. These rounds were mounted with a quartz standard (WiscSIMS in-house quartz standard: UWQ-1; Kelly et al. 2007) and coated with gold; 112 replicate analyses are presented in Supplement C4 with a two-sigma standard error of 0.3‰. Prior to oxygen isotope analysis, titanite grains were mapped by BSE and analyzed by EMP. The CAMECA IMS-1280 ion microprobe was tuned using standard operating conditions and procedures for oxygen two-isotope analyses detailed in Kita et al. (2009). The instrument used a 1.8 nA Cs+ primary beam with a diameter of 10-12 μm. Sets of 10-15 titanite analyses were bracketed by 4 analyses of

UWQ-1 (Supplement C5). Instrumental bias caused by the compositional range of Ti in the octahedral site was corrected by using the Ti concentrations from EMPA as outlined by Bonamici et al. (2015). Kita et al. (2009) and Bonamici et al. (2015) describe the SIMS methods in more detail. Spots where electron microprobe, laser ablation, and oxygen isotope analyses were taken are shown on BSE images of titanite grains in Supplement A and the $\delta^{18}O$ values are in Table 5 and Supplement C5.

Laser ablation inductively coupled plasma-mass spectrometry (LA-ICP-MS) analyses of titanite were performed at the University of Utah using a 193 nm Teledyne Photon Machines Analyte Excite laser, coupled to an Agilent 7500ce quadrupole mass-spectrometer for Na, Mg, Al, Ca, Sc, Ti, V, Mn, Fe, Zn, Ga, Rb, Sr, Y, Zr, Nb, Mo, Sn, La, Ce, Pr, Nd, Sm, Eu, Gd, Tb, Dy, Ho, Er, Tm, Yb, Lu, Hf, Ta, Pb, Th and U (Supplement C6). The laser was set to a spot size of 20-35 μm with a repetition rate of 10 Hz, laser energy of 75%, and a fluence of 1.82 j/m^2. NIST-610 synthetic glass (Norman et al. 1996; Supplement C7) was used as a standard and titanite MKED1(Spandler et al. 2016; Supplement C8) and NIST-612 (Supplement C9) were analyzed as checks. Uncertainties are typically between 5% and 10 % (except for Na (82 ppm), Mg (57 ppm), Sc (0.9 ppm), Fe (20%), Zn (10 ppm), Ga (10 ppm), Mo (2 ppm), and W (0.2 ppm)) based on replicate analyses of MKED1. Time-resolved intensity data from the ICP-MS were exported as counts per second, and element abundances were calculated offline using Iolite 2.5 (Paton et al. 2011). Si was used as the internal standard based on concentrations determined by electron microprobe analysis. Selected trace element compositions are listed in Table 3 and the entire dataset is in Supplement C6

Notch Peak pluton

The Notch Peak intrusion is the most chemically evolved of the plutons studied; it has the highest concentrations of silica and most incompatible elements (e.g., Rb, Th, U, K, and Nb). All the units form a single cluster on a TAS diagram (Fig. 2). The rocks are typically magnesian and calc-alkalic, except for two fairly altered samples. The Notch Peak magma crystallized at high fO_2 (ΔQFM ~3) as indicated by titanite and biotite compositions (Nabelek et al. 1986) and by low whole rock FeO/(FeO+MgO) ratios (Fig. 2C). Based upon Rb, Y, and Nb contents, the Notch Peak intrusion is a volcanic arc granite (Fig. 2D; Pearce et al. 1984), although the altered samples and an aplite scatter into adjacent fields. Overall, the Notch Peak granite has all the geochemical characteristics of a subduction-related silicic rock, which fits the Jurassic tectonic setting of the region (e.g., Christiansen et al. 2015). The REE patterns of the Notch Peak granite display high LREE, slight depletions in the MREE (Tb to Tm), and higher values for Yb and Lu (Figs. 2E & 2F). This is the classic REE pattern produced by titanite fractionation (e.g., Wolff and Storey 1984). Notch Peak granites typically have small negative Eu anomalies, probably because of extensive feldspar fractionation (Nabelek et al. 1986). The REE pattern for the aplites are similar to the granites, but REE contents are lower by a factor of 2 or 3 (Fig. 2E and Nabelek 1986). Compared to two-mica granites from the region, the pluton has lower $\delta^{18}O$ values (9.4‰; Nabelek et al. 1983; Lee and Christiansen 1983; Nabelek et al. 1988).

Little Cottonwood stock

The Little Cottonwood stock (LC) is more mafic (granodiorite to granite) than the Notch Peak granite (Fig. 2A) and has higher proportions of mafic minerals and titanite (~1.5%). Most samples are calc-alkalic and magnesian and fall in the volcanic arc field of Pearce et al. (1984)

This is the peer-reviewed, final accepted version for American Mineralogist, published by the Mineralogical Society of America.
The published version is subject to change. Cite as Authors (Year) Title. American Mineralogist, in press.
DOI: https://doi.org/10.2138/am-2022-8241. http://www.minsocam.org/

Like the Notch Peak granite, it crystallized at high fO_2 (ΔQFM~2-3) as indicated by titanite and Mg-rich biotite and amphibole compositions (Hanson 1995; Marsh and Smith 1997). The Little Cottonwood stock has lower Rb and other incompatible element abundances than the Notch Peak granite (Fig. 2F), as well as lower HREE concentrations. It also lacks Eu anomalies, probably because the granodiorites are less differentiated (Fig. 2E).

No whole-rock $\delta^{18}O$ values for the Little Cottonwood granodiorite have been published, but zircon has an average $\delta^{18}O$ ~5.9‰ (King et al. 2001) and using the relationship between silica content and Δ(whole rock-zircon) established by Lackey et al. (2008), the average whole rock $\delta^{18}O$ would be about 7.6‰.

Little Cottonwood enclaves

Mafic enclaves are common in the main phase of the Little Cottonwood stock and range from a few centimeters to a few meters across. Hanson (1995) concluded that the enclaves were likely cumulates ripped from the margins of the crystallizing intrusion; we re-examine this idea with new data. The enclaves have irregular, fluidal shapes and locally, form long trains that grade into highly elongate schlieren. They are porphyritic with fine-grained groundmasses; poikilitic plagioclase is the most abundant phase followed by biotite (~15%), amphibole (~12%), and titanite (~3%). Titanite poikilitically encloses other silicates in several enclaves (Sup Fig A52 & A55). Many enclaves include large megacrysts of potassium feldspar, apparently derived from the enclosing porphyritic granodiorite (Supplement Fig. A5). Quartz, apatite, zircon, and opaque oxides complete the mineral assemblage. Acicular apatite grains and quench textures indicate rapid cooling to just below the solidus temperature.

Because of low silica (50-55 wt.%) and high alkali contents, the Fe- and Mg-rich enclaves are monzodiorites on a total-alkali silica diagram (Fig. 2). In contrast to the calc-

alkaline magnesian host, they are alkalic and ferroan. They are enriched in Ti, Zr, Hf, Nb, and Y compared to the host (Fig. 2). Pb anomalies are relatively small. The enclaves also have distinctive REE patterns with higher REE contents (~2 to 3 times), higher La/Yb ratios, and deeper Eu anomalies than the host granodiorites, but they have deep Nb anomalies and Ba/Nb ratios typical of magmas from subduction settings.

TITANITE PETROGRAPHY

Titanite grains are generally wedge shaped and colorless to tan in plane-polarized light. In these intrusive rocks, they typically range from 10 μ to 1 mm long. Titanite zones can be divided into those produced by primary magmatic processes (Type 1) and those that result from post-magmatic secondary processes (Type 2). These types are further subdivided by type of zoning, and then location in the grain (core or mantle) (Table 1).

Textures of Primary Magmatic Titanite

Primary magmatic titanite is typically euhedral and displays a variety of textures. This, inclusion relationships, and its presence in phenocryst-poor volcanic rocks indicate that titanite co-crystallizes with the major mineral phases in felsic magmas ranging from dacite to rhyolite (e. g., Nakada 1991; Maughan et al. 2002). In these granitic rocks, titanite is not restricted to interstitial locations. Common inclusions are apatite and zircon, Fe-Ti oxides, quartz, and feldspars. We have identified four textural types of titanite.

Type 1U. The simplest type of titanite is unzoned or only subtly zoned in BSE images and it lacks obvious sector or oscillatory zoning (Figs. 3-5).

Types 1O and 1S. Type 1O consists of fine scale oscillating bright and dark zones in BSE images with linear boundaries mimicking the external shape of the titanite (Figs. 3-5). Individual oscillations vary in thickness from <1 μm to 5 μm. Bright oscillations are up 1.5 times

brighter than adjacent dark ones based on pixel brightness in BSE images (Supplement Fig. B2). Many oscillatory zones include BSE-bright sectors forming "fir-tree" structures that are enriched in HFSE (type 1S). These are most often found along the "spines" of grains (Supplement Fig. A7).

Type 1P. Some areas in titanite are not homogeneous or regularly zoned and instead are patchy in BSE images with irregular, variably shaped bright and dark patches that create a mottled texture. Resorbed, rounded or vermicular ilmenite inclusions are always found in these areas. We call this patchy zonation type 1P (Figs. 3-6). The outer boundaries of these patchy areas are commonly irregular, indicating uneven growth or, more likely, dissolution. The vermicular ilmenite inclusions are typically exsolved into brookite, ilmenite, and magnetite post magmatically (Fig. 6). Bauer (2015) found similar patchy areas in titanite in the Half Dome Granodiorite in central California. Broska and Petrík (2015) reported titanite surrounding earlier formed ilmenite in granites of the Western Carpathians. Both attributed the patchy texture to the result of magma mixing.

Usually, these patchy areas form distinctive cores (type 1Pc) mantled by type 1O or type 1U zones. Rarely, this patchy texture forms a thin mantle around a distinct core (type 1Pm; Fig. 5). These patchy mantles are similar in all respects to patchy cores (1Pc).

Textures of Secondary Hydrothermal Titanite

Post-magmatic titanite can form by hydrothermal processes (e.g., Mazdab et al. 2008; Xie et al. 2010; Morad et al. 2011; Liu et al. 2018; Uher et al. 2019). In BSE images, it is usually darker than magmatic titanite and has higher concentrations of F and lower concentrations of REE and other HFSE (see below).

283 **Type 2A.** Some hydrothermal (BSE-dark) titanite forms irregular anhedral rims or
284 overgrowths on magmatic titanite or magnetite (Figs. 3 & 4). These type 2A overgrowths are
285 usually unzoned but they may have oscillations or mottling.

286 **Type 2B.** Commonly, small, thin, linear, and BSE dark grains of hydrothermal titanite
287 form along cleavage planes of biotite altered to chlorite (Fig. 3B) indicating the role of lower-T
288 fluids flowing along permeable cleavages (Supplement Figs. A38, A45, A47, & A48). Secondary
289 titanite of this type 2B is very common in plutonic rocks (e.g., Xie et al. 2010; Morad et al. 2011;
290 Kontonikas-Charos et al. 2019). Replacement of magmatic biotite by hydrothermal titanite may
291 be explained by the loss of Ti from biotite during chloritization and the loss of Ca by dissolution
292 of plagioclase during alteration. Analysis by laser ablation and even by electron microprobe is
293 difficult because the grains are typically small (<5 μ), anhedral, and intimately intergrown with
294 the surrounding biotite/chlorite.

295 **Type 2F.** Aplite dikes and sills associated with the Notch Peak pluton have a distinctive
296 hydrothermal titanite with high Fe content, which typically forms on grain tips or as thin
297 overgrowths (Supplement Figs. A22 & A23). This type is bright in BSE images due to the high
298 Fe content and not due to high REE content.

299 **Type 2T.** In the Notch Peak pluton, some secondary titanite replaces magmatic titanite
300 while maintaining the shape of the original grain. Type 2T appears in BSE images as areas of
301 darker, often mottled titanite that crosscut magmatic zonation (Fig. 4A; Supplement Figs. A18 &
302 A19).

303 **Type 3R.** If secondary alteration is extensive, some titanite grains are completely
304 replaced by masses of bladelike rutile or brookite, calcite, quartz, magnetite, Nb-Ta-Ti oxides,
305 and fluorides that retain titanite's wedge-like shape (type 3R, Fig. 7, Supplement Fig. A17).

306 Complete replacement like this has been observed in other granites (*e.g.*, Broska et al. 2007,
307 2015; Middleton et al. 2013).

308 **Titanite Textures in the Notch Peak and Little Cottonwood Intrusions**

309 Titanite grains in the Notch Peak pluton are generally euhedral and range from 50 to 200
310 μ across. They typically make up around 0.9% of the granite (Figs. 4 & 7). We examined 66
311 titanite grains from six different localities in granite and two in aplite (Fig. 1). A few grains
312 (<20%) have areas that are unzoned (type 1U textures), but most grains (~90%) have large
313 oscillatory growth zones (1O) usually associated with sector zones (1S) (Fig. 7). In two samples
314 (NB-100 and NP-3; Supplement Fig. A13) from the eastern margin of the pluton almost 30% of
315 the grains have patchy cores with ilmenite inclusions (type 1Pc). No other samples from Notch
316 Peak pluton have these patchy cores. Anhedral grains or overgrowths of hydrothermal titanite
317 (2A) were found on or near 18% of the grains, while secondary titanite replacing primary
318 magmatic titanite but maintaining the shape of the original grain (type 2T) was found in only two
319 samples—NP-1 and NP-6 (Fig. 4 and Supplement Figs. A6 & A18). In these two samples, about
320 68% of the titanite grains are type 2T. Titanite formed in altered biotite (2B) is common, but we
321 were unable to obtain LA-ICP-MS or EMP analyses because the grains were too small. In two
322 samples, NP-2 and NP-5, many titanite grains (type 3R; Fig. 7) were partially or completely
323 replaced by aggregates of secondary minerals (rutile or brookite, biotite, quartz, Ti-poor
324 magnetite, ilmenite (some with MnO up to 28 wt.%), and various Nb-Ta-Ti oxides probably of
325 the aeschynite or euxenite groups), monazite, and Ca-REE-Y fluorides. In these two samples, no
326 hydrothermal titanite was found.

327 Titanite in the Little Cottonwood stock forms large subhedral to euhedral magmatic
328 grains ranging from 100 μm to over 1 mm long. Titanite is more abundant (1.5%) here than in

329 Notch Peak pluton. We examined 111 grains from the stock. Of these, 44 had distinct cores with
330 37 (33%) having patchy (type 1Pc) cores with abundant resorbed ilmenite inclusions that have
331 exsolved to assemblages of rutile/brookite, magnetite, and Mn-rich ilmenite (Fig. 6). Such patchy
332 cores are not found in samples from the southwestern margin of the pluton (samples CC and LC-
333 27). Oscillatory zones (1O) almost always mantle these cores. Dissolution surfaces, indicated by
334 wavy borders that truncate existing zoning, are common at the core-mantle boundary and
335 between some oscillatory zones (Fig. 5; Supplement Figs. A34 to A53). Outside of the patchy
336 cores, titanite may contain inclusions of magnetite, apatite, and zircon, although magnetite is
337 usually on the margins of the grains, not within them. Inclusions of the major silicate minerals
338 are rare and patchy mantles (1Pm) are absent. About 30% of titanite grains in the Little
339 Cottonwood stock have either BSE-dark rims or irregular extensions between feldspars and
340 quartz (type 2A, Fig. 3). Some titanite forms glomerocrystic clusters (Supplement Fig. A36).
341 Secondary titanite forms blade-like replacements along cleavage traces in chloritized biotite
342 (type 2B) where it contacts magmatic titanite and in areas close to magmatic titanite (Fig. 3).
343 Titanite in the mafic enclaves in the Little Cottonwood granodiorite forms either large
344 (200 μm -2 mm) irregular masses, poikilitic grains, or euhedral grains similar to those in the
345 main stock (Supplement Figs. A54-A87 & B14). Titanite is much more abundant in the enclaves
346 (3.0 vol.%) than in the host. We examined 233 grains or glomerocrysts in nine different enclaves
347 from three samples. Glomerocrysts of titanite (Supplement Figs. A65, A67, A77), where each
348 subcrystal has its own distinct zoning pattern, are common in the enclaves while rare in the host
349 granodiorite. In many enclaves, titanite crystallized late, and contains large poikilitic inclusions
350 of plagioclase and hornblende or grew as anhedral masses surrounding oxide cores (Supplement
351 Figs. A68, 72,73, 74 & 82). Over 40% of grains examined had the poikilitic texture, but

proportions are quite variable. For example, in sample CH-153A, 90% of the titanite grains are poikilitic, while in sample CH-153D, collected a few meters away, only 10% of the titanite grains are poikilitic. In the enclaves, secondary titanite occurs as BSE-dark anhedral overgrowths (type 2A) on ~20% of grains and as irregular extensions into chloritized biotite (type 2B) around ~6% of grains (Fig. 5). Non-poikilitic titanite grains in the enclaves typically have simple unzoned or patchy cores (1U & 1Pc) with bright sectors (1S) traversing their central parts. Inclusions of apatite and zircon are common. A few have mantles with distinct oscillatory zoning patterns (Supplement Fig. A65, 66, 67, & 77). Patchy cores (type 1Pc) are in ~28 % of the grains examined. Irregularly shaped ilmenite inclusions that are now exsolved and altered are just like the 1Pc cores in many parts of the Little Cottonwood granodiorite (Supplement Figs. A62- 66, 68, 75-78, & 80). A unique type of titanite found only in four of the nine enclaves has patchy mantles (type 1Pm) (Supplement Figs. A67 & 75) otherwise identical to patchy cores.

GEOCHEMISTRY OF TITANITE

Titanite in the Notch Peak pluton

The composition of magmatic titanite in the Notch Peak granite falls within the range of magmatic titanite as summarized in Kowallis et al. (2018). For example, substitutions for Ca and Ti are about 0.1 apfu and Fe/Al ratios are close to 1 (Tables 2, 3, and 4). Unzoned, oscillatory, and bright sector zones (types 1U, 1O, & 1S) have similar REE patterns with LREE (La, Ce, Pr, Nd) showing the greatest enrichment relative to chondrite (e.g., Colombini et al. 2011), a rise from La to Ce, negative Eu anomalies, and leveling off in heavy REE (Figs. 4 & 8; Supplement Fig. B8). Negative Eu anomalies reflect Eu-depletion in the parental magma and lower compatibility of Eu^{2+} in titanite. As expected, BSE-bright sector zones (type 1S) are richer in

most trace constituents than unzoned and oscillatory types, except for Mn (Fig. 8; Supplement Fig. B5). Magmatic titanite throughout the pluton is compositionally similar, but titanite in NP-1 on average has lower REE and higher F (Fig. 9).

Compared to magmatic titanite, hydrothermal titanite (2A, 2T) typically has higher concentrations of F, Mg, Mo, V, and U, along with lower Th/U ratios (Fig. 8; Supplement Fig. B15). Hydrothermal titanite has lower concentrations of most other trace elements, including the REE (Tables 2, 3, and 4; Figs. 8, 10C, 11 & Supplement Figs. B8 & B9). F concentrations are about 2 times higher in hydrothermal titanite, but Al is not higher (Fig. 10) as it commonly is in hydrothermal titanite elsewhere (Kowallis et al. 2018). REE concentrations, except La, are lower by as much as a factor of 8, especially the middle to heavy REE (Fig. 4, 8, 11, & 12). Unlike magmatic titanite, Eu anomalies are absent. Th is typically depleted in the hydrothermal titanite, but U is enriched resulting in low Th/U ratios (Figs. 8 & 11; Supplement Fig. B15). Perhaps the most striking compositional difference is the strong depletion of Ta in post-magmatic titanite (Fig. 8), which is 4 to 5 times lower in concentration than in magmatic titanite. Nb is also depleted, but not as much—about 1 to 2 times. Thus, hydrothermal titanite has relatively high Nb/Ta ratios. Despite the depletions of these HFSE, Zr and Hf have about the same concentrations in both magmatic and hydrothermal titanite (Fig. 11), indicating similar crystallization temperatures.

Titanite-bearing aplite dikes and sills are common in and near the Notch Peak pluton. Nabelek (1986) found that the aplites are “depleted in Ba, Sr, and the REEs, while the concentration of highly charged elements, Zr, Ta, Hf, Th, and U, is about the same as in the major lithologic units in the stock.” He concluded that the aplites crystallized from melt saturated with a Cl-rich hydrothermal fluid. This conclusion is supported by the fact that titanite in the

aplites has similar textural types as in the rest of the pluton (oscillatory, bright sectors, unzoned, and secondary) as well as similar major element compositions and temperature dependent Zr concentrations. However, magmatic titanite in the aplites has higher F concentrations and distinct REE patterns with lower overall REE totals, deeper Eu anomalies, and middle REE (Gd-Er) depletions (Figs. 8 and 10) consistent with the overall lower concentrations of REE in the aplites compared to the granite. Titanite in the aplites has very low Th/U ratios (<2; Supplement Fig. B15) compared to other igneous titanites, making them more akin to metamorphic or hydrothermal titanite (Abraham et al. 1994).

Hydrothermal titanite in the aplites has REE concentrations lower than magmatic titanite and lacks Eu anomalies, but Zr concentrations are not distinctly different from magmatic titanite (Figs. 8 and 11). All these features are similar to hydrothermal titanite in the main part of the pluton. However, titanite in the aplites is more variable in composition; the average composition of the various types of titanite in the Little Cottonwood stock generally form distinct clumps or simple trends, while the average compositions of titanite types in the Notch Peak aplites scatter or cut across the other trends (Fig. 10). In addition, the high-Fe titanite (type 2F) that typically is found on tips of grains or as thin overgrowths (Supplement Figs. A22 to A25) has average Fe/Al of 2.1, considerably higher than for Notch Peak titanite (1.0 to 1.1) or the other aplite types (0.9 to 1.2) and falls off the LREE-Fe/Al plot (Fig. 10D). This high-Fe titanite typically has strong positive Eu anomalies (Fig. 8). Compared to other types of hydrothermal titanite in the aplites, the average high-Fe type is relatively depleted in LREE, enriched in mid to heavy REE, as well as Y, Mo, Sn, F, and Hf (Fig. 11).

421 **Titanite in the Little Cottonwood stock**

422 Primary magmatic titanite in the Little Cottonwood granodiorite has high Ti (>0.88 apfu)
423 and Ca, and low Fe, F, and Y compared to Notch Peak titanite (Figs. 10 & 11; Tables 2, 3, and
424 4). Fe/Al ratios are lower than in magmatic titanite of the Notch Peak intrusion (Fe/Al=0.89
425 versus Fe/Al=1.03; Fig. 10). Little Cottonwood titanites have REE patterns like those in other
426 igneous rocks in that they are LREE enriched and have La/Ce_N <1 (Figs. 8 & 11, Table 4;
427 Supplement B10). Types 1S, 1O, and 1U titanites have negative Eu anomalies. In contrast,
428 patchy cores (1Pc) have very small negative to large positive Eu anomalies (Fig. 12). The patchy
429 cores with positive Eu anomalies (1Pe) also have relatively low concentrations of other REE.
430 Little Cottonwood titanites are also distinctly depleted in HREE-Y compared to Notch Peak. The
431 patchy cores (type 1Pc) are the most depleted (Fig. 11; Supplement Fig. B1). Sector zones (type
432 1S), the brightest zones in BSE images, have higher Zr and light to middle REE and lower F
433 contents when compared to darker patchy cores, unzoned cores and mantles, or oscillatory zones
434 (Figs. 10, 11, & 13; Table 4). The compositions of titanite from the southwestern Little
435 Cottonwood stock (samples LC-CC and LC-27; Fig. 1) typically overlap titanite in the rest of
436 Little Cottonwood stock in all elements, but trend slightly toward higher in Ca and lower in REE
437 and Fe (Fig. 9).

438 Hydrothermal titanite replacing magmatic titanite (2T) is rare in the Little Cottonwood
439 stock (only a few spots were found in LC-HFT). However, anhedral/overgrowth titanite (type
440 2A) is common and, like secondary titanite in the Notch Peak granite, tends to be BSE-dark and
441 have low concentrations of most trace elements compared to magmatic titanite, including Na,
442 REE (especially medium to heavy REE), Zr, Hf, Nb, and Ta, while incorporating higher
443 concentrations of F, Al, Mg, and U (Figs. 11, 13, and Supplement Fig. B10 &B11). Titanites of

type 2A also have different REE patterns compared to magmatic titanite with less rise from La to Ce, no negative Eu anomalies, and significantly lower Nd/Er ratios indicating stronger depletions of the MREE and Y (Fig. 12). Hydrothermal titanite generally has lower Th concentrations and consistently higher U, yielding the characteristic low Th/U ratios (<2; Supplement Fig. B15). Titanite that replaced or grew in close association with biotite (type 2B) formed very small crystals allowing only 9 laser ablation spots and 7 electron microprobe spots to be analyzed. These revealed that type 2B has the lowest concentrations of Ti and REE of any type studied and strong positive Eu anomalies like those found in hydrothermal titanite by Kubeš et al. (2021). Type 2B also has the highest F, Al, and lowest Fe/Al of any Little Cottonwood type (Figs. 10 & 12). Hydrothermal titanite in the Little Cottonwood granodiorite also has Nb and Ta depletions and high Nb/Ta ratios, like those found in Notch Peak titanite (Fig. 12).

Titanite in the Little Cottonwood enclaves

Compositions of magmatic titanite in the Little Cottonwood enclaves are very similar to titanite in the host granodiorite but less variable, with slightly higher average Ti (by about 0.01 apfu; Fig. 10; Table 2). Trace element concentrations (Table 4) and REE patterns are also like those in titanite in the host granodiorite with LREE enrichments ($La/Yb_N \sim 40$) and negative Eu anomalies (Fig. 12). However, some grains lack Eu anomalies or have positive Eu anomalies, even in magmatic titanite (Fig. 12; Supplement Fig. B12). Positive Eu anomalies in some patchy titanite zones (types 1Pc & 1Pm) are similar to but not as large as those in the unusual type 1Pe zones in the host. Poikilitic titanite grains typically lack Eu anomalies (type 1Up; Fig. 11). Unzoned poikilitic titanite also has lower concentrations of REE and higher F than other magmatic types, but not as low as secondary titanite (type 2A), which is the lowest of the types in REE and highest in F and U (Figs. 12 & 13; Supplement Fig. B13 & B15). HREE are more

467 depleted than the LREE (Fig. 12). Hydrothermal titanite in the enclaves shares other key
468 characteristics with titanite hosted in the granodiorite, including high Al (Fig. 10), small negative
469 or even positive Eu anomalies (Fig. 12), as well as high Nb/Ta and low Th/U ratios (Fig. 13). We
470 have no analyses of hydrothermal type 2B titanite from the enclaves because of its small grain
471 size.

472 **ZR- GEOTHERMOMETRY AND AL-BAROMETRY**

473 Zr concentrations in titanite have been used to estimate temperatures of crystallization
474 using the pressure-sensitive geothermometer of Hayden et al. (2008). We assumed $a\mathrm{TiO_2} = 0.75$
475 for all samples. A change of 0.1 GPa only yields a difference of ~10°C, well within variations
476 caused by analytical uncertainty for Zr. Erdman et al. (2019) calibrated an empirical
477 geobarometer based on the Al_2O_3 concentrations in magmatic titanite in equilibrium with
478 amphibole, plagioclase, K-feldspar, quartz, biotite, and magnetite ± ilmenite.
479

480 **Notch Peak granite and aplites**

481 The crystallization pressure for the Notch Peak granite is estimated to be between 0.1 and
482 0.2 GPa based on a stratigraphic reconstruction by Nabelek et al. (1986); we chose a fixed
483 pressure of 0.15 GPa. The Al-in-titanite geobarometer of Erdman et al. (2019) gives an average P
484 of 0.198 ± 0 .014 GPa based on the average Al_2O_3 content of 1.36 ± 0.14 wt.% in the titanite.
485 The average zircon-saturation temperature (Boehnke et al. 2013) calculated from whole rock
486 compositions is 767°C ± 11. Zr-in-titanite temperatures are lower (Fig. 14; Supplement C10).
487 Magmatic titanite (1U and 1O) yields a temperature range of 792° to 684°C with an average of
488 718°C ± 21 (n=61). Overall, these magmatic titanite temperatures correlate positively with REE
489 contents (La-Yb as determined by LA-ICP-MS) (Fig. 14) and negatively with U, F, and Eu.

Hydrothermal titanite (2T and 2A) yields a range of temperatures from 740° to 660°C with a somewhat lower average of 711°C ± 22 (n = 12). A t-test indicates these average temperatures are statistically different. Hydrothermal titanite also has lower REE contents than magmatic titanite (Fig. 14).

In the Notch Peak aplites, temperatures for magmatic titanite range from 751° to 694°C with an average of 734°C ± 14 (n=12), which is higher than but overlaps with temperatures from titanite in the granite. However, temperature (or Zr content) is poorly correlated with REE concentrations, which are lower than in titanite in the main intrusion. Temperatures for hydrothermal titanite in aplite range from 748° to 650°C, with an average of 690°C ± 31 (n=9), about the same as hydrothermal titanite in the granite. The high-Fe titanites (type 2F) in the aplites have an average temperature of 718°C ± 34 (n=4), but they have low REE contents (that do not correlate with Zr-in-titanite temperatures) consistent with a post-magmatic origin (Fig. 14).

Little Cottonwood stock

Determining pressure for crystallization of the Little Cottonwood stock is difficult as it was exposed during flexural-isostatic uplift associated with the Wasatch normal fault, which produced a regional tilt to the east. As such, it probably crystallized at pressures ranging from 0.31 to 0.17 GPa decreasing to the east (John 1989; Parry and Bruhn 1987). The Al-in-titanite geobarometer does not reproduce this pressure range or a systematic trend across the pluton; the overall average P is 0.190 ± 0.017 GPa based on an average Al_2O_3 content of 1.29 ± 0.10 wt% (n = 1513) for magmatic titanite.

To calculate Zr-in-titanite temperatures, we assumed the pressure of crystallization was 0.25 GPa for the middle of the pluton (LC-36, LC-HFT, and LC-TQ) and 0.19 GPa for the

eastern part of the pluton (LC-23, LC-SB, and LC-SL). The average zircon-saturation temperature is 769°C ± 17 (Supplement C10). Magmatic titanite (1U, 1O, 1Pc, and 1Pm) temperatures are lower (average 719° ± 26°C, n = 138), but increase with increasing REE content (Fig. 14). Patchy and unzoned titanite (1Pc & 1Pm, and 1U) typically yield slightly higher temperatures (730°C ± 36° (n=32) and 721°C ± 17 (n = 29)) than oscillatory zoned titanite (1O) at 709°C ± 13° (n = 45). BSE bright sector zones (1s) had an average temperature of 726°C ± 11°. These temperatures are similar to other estimates of crystallization temperature. Hanson (1995) calculated temperatures from coexisting plagioclase and hornblende of 707-736°C and Stearns et al. (2020) found a range of 650-800°C with a mode of 725°C using Zr-in-titanite (747°C when recalculated with $a\mathrm{TiO_2}$ of 0.75). Hydrothermal titanite (2A) temperatures range from 600°C to 720°C and correlate strongly with REE content (average T = 674°C ± 33 (n = 39). Hydrothermal titanite with strong positive Eu anomalies and the lowest REE contents (Fig. 14) is almost always intergrown or associated with biotite (type 2B) and extends to the lowest temperatures (734° to 597°C).

Little Cottonwood enclaves

Magmatic titanite in mafic enclaves from the Little Cottonwood stock yields an average Zr-in titanite temperature of 731 ± 30° (n = 48) somewhat higher than for titanite in the host granodiorite (718 ± 16°C). However, patchy cores (1Pc) in the enclaves had a much higher average temperature at 759°C ± 44 (n = 12) and ranged from 714 to 834°C. There is very little secondary titanite in the enclaves, but the average temperature was 689°C ± 39 (n=9), somewhat lower than for the magmatic titanite.

.

This is the peer-reviewed, final accepted version for American Mineralogist, published by the Mineralogical Society of America.
The published version is subject to change. Cite as Authors (Year) Title. American Mineralogist, in press.
DOI: https://doi.org/10.2138/am-2022-8241. http://www.minsocam.org/

OXYGEN ISOTOPIC COMPOSITION OF TITANITE

Experiments show that magmatic titanite is one of the first minerals that closes to oxygen diffusion during cooling and that it is fairly retentive of magmatic $\delta^{18}O$ values (King et al. 2001; Zhang et al. 2006; Bruand et al. 2019). Thus, $\delta^{18}O$ values may reflect original growth conditions and may shed light on pluton origin and hydrothermal alteration (King et al. 2001; Bonamici et al. 2014). High $\delta^{18}O$ may indicate magmatic origins. Lower or even negative $\delta^{18}O$ values for hydrothermal titanite are consistent with hydrothermal alteration involving low $\delta^{18}O$ meteoric water (e.g., Bonamici et al. 2011; Bonamici et al. 2014). Representative BSE images of titanite grains (oNP-1) and (oHFT-7) are in Figure 15, along with $\delta^{18}O$ values and temperatures calculated from Zr concentrations (see also Supplement Fig. B7).

$\delta^{18}O$ in Notch Peak magmatic titanite, including the aplites, ranges from 5.7‰ to 6.4‰ and has an average of 6.0 ± 0.3‰ (n = 28; Table 8). King et al. (2001) found a $\delta^{18}O$ of 6.4‰ on titanite separated from our sample NP-1. The average $\delta^{18}O$ (6.2 ± 0.3‰ (n = 6) of hydrothermal titanite (2A & 2T) is statistically indistinguishable according to a t-test implying a magmatic origin for the hydrothermal fluid.

Magmatic titanite (1C, 1U) in the Little Cottonwood granodiorite has an average $\delta^{18}O$ of 4.9‰ ± 0.4 (n = 78). There are no obvious differences in the oxygen isotopic composition of titanite from various parts of the intrusion (i.e, east vs west) or in the various textural types of magmatic titanite. Even the distinctive patchy cores (1Pc) with their higher REE and Zr-temperatures are indistinguishable from the other types (Fig. 16). In contrast, hydrothermal titanite (type 2A) ranges from 1.7 to 5.2‰ and has an average $\delta^{18}O$ of 4.6‰ ± 0.5 (n = 7). Titanite in chloritized biotite (type 2B; Figs. 3 & 15) has a significantly lower average $\delta^{18}O$ of 3.1‰ ± 1.2 (n = 5). Some grains in chlorite in LC-HFT have $\delta^{18}O$ as low as 1.7‰. These

558 relatively low $\delta^{18}O$ values indicate involvement of meteoric water in the formation of chlorite
559 from biotite and associated titanite. (At high altitudes in temperate climates $\delta^{18}O$ in meteoric
560 water may be as low as -5 or -10‰.) King et al. (2001) found mineral separates of green
561 hydrothermal titanite from the Little Cottonwood stock had an average $\delta^{18}O$ of 1.3‰ compared
562 to 4.6‰ for magmatic titanite.

563 Overall, the $\delta^{18}O$ of magmatic titanite in the Little Cottonwood granodiorite (4.9‰) is
564 about 1.1‰ lower than that in the Notch Peak granite (6.0‰), probably because of different
565 compositions of the parent magmas. $\delta^{18}O$ values for whole rock samples of the Notch Peak
566 granite range from 8.9 to 10.2‰ and average 9.4 +/- 0.4‰ (Nabelek et al. 1983). The whole
567 rock $\delta^{18}O$ values for the Little Cottonwood granodiorites should be about 7.6‰ or about 1.8‰
568 lower than the typical Notch Peak granite, as estimated from the zircon composition (5.9‰; King
569 et al. 2001) and the Δ(WR-zircon) model of Lackey et al. (2008).

570 Magmatic titanite in mafic enclaves has oxygen isotope values similar to those in the rest
571 of the complex (Fig. 16). Magmatic titanite (types 1U, 1Pc) has an average $\delta^{18}O$ of 5.1 ± 0.3‰
572 (n = 43) (Table 5; Fig. 16). Patchy titanite cores (1Pc) are indistinguishable with a mean $\delta^{18}O$ of
573 5.1‰ ± 0.2 (n = 7).

574 ## TITANITE CRYSTALLIZATION HISTORIES

575 We outline the crystallization history of titanite in the two plutons studied here (Figs. 17
576 & 18) to answer the questions posed in the introduction.

577 ### Crystallization of Titanite in the Notch Peak Pluton

578 A simplified history of the titanite in the Notch Peak granite is sketched in Figure 17.
579 Following emplacement at a shallow level, titanite co-crystallized with other phenocrysts (Fig.
580 17A). The cup-shaped REE patterns of the granite (Fig. 2) show that previous titanite crystallized

and was removed from the magma (Nabelek et al. 1986). Cores bounded by dissolution surfaces (Fig. 17B) have REE patterns and major element compositions like surrounding parts of the grains, indicating they crystallized from the same or a very similar melt rather than as a result of mixing with another melt. BSE-bright sector zones (Figs. 4, 7, and 17C) are enriched in REE-Y and Zr, as well as Fe, Mn, Mo, and Sn.

Oscillatory zoned mantles are typically similar in overall composition and in REE patterns, to cores (type 1U) (Figs. 4, 12, & 15). These rings are thin and range between 5-10 μm across. Melnik and Bindeman (2018) hypothesized that these oscillations could be the result of changes in partition coefficients for highly compatible elements like Zr and REE due to small ~5° C temperature oscillations. However, the concentrations of these elements in adjacent laminations may be different by factors of 3 to 5 (Supplement Figs. B2 & B3). It seems unlikely that such small changes in T could more than triple trace element partition coefficients. More likely, differing crystal growth and diffusion rates of elements in the melt created an oscillating disequilibrium system that yielded REE-rich, BSE-bright bands alternating with REE-poor, F-rich, BSE-dark zones (Paterson and Stephens 1992; Shore and Fowler 1996; Melnik and Bindeman 2018). Euhedral magnetite, zircon, and apatite occur as inclusions in or on the margins of titanite but are not as common or resorbed as ilmenite in the patchy zones of titanite from Little Cottonwood stock.

In short, euhedral shapes, magmatic zoning patterns, elemental composition (e.g., high REE and low F), high Th/U ratios, and high $\delta^{18}O$ values (6.0‰) show that most of the titanite originated as magmatic crystals, in contrast to the suggestion of Nabelek et al. (1986) that titanite formed because of biotite breakdown.

603 However, hydrothermal titanite replacing biotite (2B) does form arrays of small, spike-
604 like grains that are aligned along cleavages in chloritized biotite. Some titanite also crystallized
605 from hydrothermal fluids to form anhedral overgrowths and interstitial extensions (type 2A); in
606 places, this hydrothermal titanite replaced magmatic titanite (type 2T) (Figs. 4 & 17E). These
607 secondary types are typically unzoned or mottled and darker in BSE images. They have lower
608 concentrations of relatively insoluble HFSE like Nb, Ta, and the REE (Fig. 11). The high Nb/Ta
609 ratios of the hydrothermal titanite are likely the result of the greater solubility of Nb in
610 hydrothermal fluids (Chen et al. 2018); thus, fluids and the titanite precipitated from them should
611 be Ta-poor. Various Ta-Nb-Ti minerals, probably rutile, brookite, and aeschynite/euxenite,
612 formed during alteration of magmatic titanite and retained Ta relative to Nb. Despite having
613 lower REE contents, the negative Eu anomalies of magmatic titanite were erased in hydrothermal
614 titanite during equilibration with fluid (Fig. 4 & 8); perhaps the fluids were oxidized, and Eu was
615 dominantly in the +3 state and behaved like other REEs.
616 The hydrothermal titanite also has higher F, Mg, Mo, V, and U contents (Fig. 8; Table 4).
617 The enrichments are probably the result of the greater solubility in fluid. For example,
618 concentrations of insoluble Th in hydrothermal titanite are lower than in the primary titanite and
619 concentrations of soluble U are higher, creating low Th/U ratios (<2), which are typical of
620 hydrothermal titanite formed in oxidized environments where U^{6+} is highly mobile (e.g.,
621 Abraham et al. 1994). Kowallis et al. (2018) found similar depletions in REE and enrichment of
622 F in secondary rims of titanite in other plutonic rocks. These significant compositional changes
623 are not usually found in volcanic titanites with their shorter crystallization histories and lack of
624 post-magmatic titanite.

In the Notch Peak granite, the $\delta^{18}O$ of the hydrothermal titanite is indistinguishable from that of the magmatic titanite (6.0‰ vs. 6.2‰; Table 5; Fig. 15), showing that the hydrothermal fluids exsolved from the magma and had little if any meteoric component. Nabelek et al. (1983) came to the same conclusion using whole rock and major mineral O and H isotopes. Zr concentrations and calculated temperatures (average 711°C) are somewhat lower than for magmatic titanite (718°C), but higher than expected for titanite formed by hydrothermal alteration involving heated meteoric water. Nabelek et al. (1983) estimated that chloritization, which is contemporaneous with formation of type 2B titanite, occurred at about 600°C in the presence of magmatic fluid.

In some parts of the Notch Peak pluton, post-magmatic, oxidative hydrothermal alteration has partially or completely replaced titanite with TiO_2 (rutile or brookite), ilmenite, monazite, biotite, quartz, and magnetite, forming skeletal structures with the same shape as the original titanite grain (type 3R; Fig. 17F; Fig. 7).

Aplites associated with Notch Peak pluton have distinctive whole-rock compositions but, like the main stock, seem to have fairly simple crystallization histories. The first formed titanite in the aplites is typically unzoned or weakly oscillatory, with significant bright sectors. Titanite in the aplites is REE-depleted compared to that in the granites; this reflects the REE-depleted composition of the aplite magma (Fig. 2, 8, & 11; Nabelek, 1986). Negative Eu anomalies are deeper than in titanite in the granite (Fig. 8), attesting to more differentiation involving the removal of feldspars to form the aplite magma. F-enrichments are probably caused by the enhanced magmatic evolution as well. However, Zr and Hf are not depleted as they are in many evolved magmas. We interpret this to mean that their abundances are controlled more by magma temperature; Zr-in-titanite temperatures are higher or about the same as in the granite (average

734°C vs. 718° for magmatic titanite in the granite). The low Th, high U, and low Th/U ratios (<2) in the magmatic titanites from the aplites are more like hydrothermal titanite than other magmatic titanites (Supplement Fig. B15). We suggest that this is because the aplites crystallized from a fluid-saturated magma, as initially proposed by Nabelek (1986).

Some titanite grains in the aplites were also affected by post-magmatic secondary processes that overprinted magmatic zonation. Compared to magmatic titanite, hydrothermal titanite is even more enriched in F and more depleted in REE, but not in Zr or Hf. Zr-in-titanite temperatures average 690°C. All these features suggest involvement of magmatic fluid in the origin of the secondary titanite in the aplites. Just like the hydrothermal titanites in the main intrusion, this titanite also lacks Eu anomalies (Fig. 11). The further depletion of REE, destruction of negative Eu anomalies, and enrichment in F may be an indication that the fluid had relatively low concentrations of less soluble REE and higher concentrations of more soluble F. In addition, thin rims and tips on a few titanite grains are enriched in Fe (0.08 apfu) and even more depleted in REE (Fig. 11). These grains typically have positive Eu anomalies (Fig. 11), probably as a result of the contemporaneous break down of Eu-rich feldspars as the late titanite formed. Nabelek (1986) concluded that the aplites crystallized from magma saturated with a Cl-rich fluid. Given the affinity of Cl to complex with Fe, these late Fe-enriched hydrothermal titanites should be expected.

Crystallization of Titanite in the Little Cottonwood Stock

Titanite in the Little Cottonwood stock has more diverse zoning than that in the Notch Peak granite. It also contains mafic enclaves indicating a more complex crystallization history. Based on the physical and chemical evidence outlined above, we conclude that the mafic enclaves formed by mixing a hotter and more mafic magma with felsic magma (Fig. 18). Their

671 fluidal shapes, quench textures (including elongate apatite), apparent exchange of phenocrysts,
672 titanite enrichment, alkaline and ferroan compositions (Fig. 2), and negative Eu anomalies (Fig.
673 2) are inconsistent with an origin as cumulates as proposed by Hanson (1995). Moreover, the
674 evidence for ilmenite rounding and resorption as fO_2 increase (accompanied by titanite
675 crystallization), the high Zr, Hf, and calculated temperatures for the early patchy cores with their
676 positive Eu anomalies and low REE (indicating simultaneous plagioclase dissolution) also are
677 consistent with a magma mixing origin for the enclaves. Nonetheless, Hanson (1995) showed
678 that plagioclase, biotite, and hornblende in the enclaves have the same compositions as they do
679 in the granodiorite host. Thus, if mixing occurred, the enclave minerals must have diffusively
680 equilibrated with those in the host. Moreover, it is possible that some residual liquid may have
681 been expelled from the enclaves as they solidified. As a result of these changes, major and trace
682 element compositions of the enclaves were greatly modified and may only grossly reflect the
683 composition of the mafic end member (as outlined by Christiansen and Venchiarutti (1990) for
684 enclaves in rhyolites). For example, the normalized trace element diagram for the whole rocks in
685 Figure 2F is unusual, with high concentrations of REE but lower concentrations of Ba, Rb, K,
686 elements that are typically more enriched in alkaline magmas with similar REE concentrations.
687 Titanite has low alkali contents but high REE contents. It seems that the trace element pattern is
688 strongly controlled by the abundance of titanite in the enclaves, which is ~ 3%.

689 Thus, we conclude, that during one major, or possibly several minor magmatic recharge
690 events, a hotter, reduced, ilmenite-magnetite-bearing, titanite-free mafic magma (Fig. 18A)
691 mixed with a cooler, more oxidized, felsic, and calc-alkaline magma. Mixing and consequent
692 oxidation caused ilmenite in the mafic magma to become unstable and partially resorb into the
693 melt (Fig. 18B; McLeod et al. 2011; Bauer 2015; Jiang et al. 2016; Zhao et al. 2021). This

694 resulted in the rounded anhedral grains of ilmenite found in the patchy cores of many titanite
695 grains. As the hybridized, but still mafic, magma continued to mix with felsic magma, it became
696 more oxidized and silicic, and titanite crystallized on the resorbed ilmenite grains; Piccoli et al.
697 (2000), McLeod et al. (2011), and Bauer (2015) have linked similar textures with titanite
698 replacing ilmenite to changes in oxygen fugacity. During this dynamic mixing stage, patches of
699 various composition formed, dissolved, and formed again to create the patchy zones (1Pc; Fig.
700 18C). Zr and Hf are enriched in these patchy cores (Fig. 11) resulting in Zr-in-titanite
701 temperatures of 760° to 730°C with an average of 731°C; titanite temperatures in the host granite
702 average about 715°C. Moreover, the dissolution of Eu-rich but REE-poor plagioclase during
703 mixing and crystallization of the patchy titanite cores is indicated by the positive Eu anomalies
704 and low REE contents in 1Pc zones (Fig. 12). Resorption of plagioclase and ilmenite probably
705 released the Ca, Si, and Ti needed to form titanite. As the dynamic mixing subsided, euhedral
706 oscillatory rims (1O) with contemporaneous sector zones formed mantles on the patchy cores
707 (Fig. 18D & 18E). Intervening dissolution surfaces might reflect repeated infusions of mafic
708 magma or convective movement of titanite into hybridized zones of varying composition and
709 temperature. Some euhedral grains of titanite in the enclaves have cores (1U) mantled by patchy
710 oxide-rich zones (1Pm) indicating that more than one magma mixing event occurred. In the
711 enclave magma, some titanite crystallized late, after hornblende and plagioclase and pokilitically
712 enclosed them. As the mafic melt cooled and crystallized during quenching, silica activity
713 eventually became high enough and temperature low enough to stabilize titanite in the evolved
714 residual liquid. This poikilitic titanite lacks negative Eu anomalies, perhaps a characteristic of the
715 mafic magma. However, quenching during mixing with the lower T felsic magma preserved the
716 euhedral shapes of most of the grains. In the few coarser enclaves, titanite grains are anhedral

717 with rims grown into and molded around the surrounding silicates (Supplement Figs. A68, A72,
718 A74 & A82) suggesting that titanite continued to grow from mushy magma with only a few
719 percent of melt remaining.

720 Zr-in-titanite temperatures in the granodiorite (~720°C) are similar to those derived for
721 other minerals like zircon (650-800°C; Ti-in-zircon, Stearns et al. 2020) and plagioclase-
722 hornblende (707-736°C; Hanson 1995), consistent with the textural interpretations showing that
723 titanite is not restricted to late-stages of crystallization in the granodiorite. Early patchy cores in
724 the enclaves crystallized at an average temperature of 759°C, but the average T of all the titanite
725 in the enclaves is 731°C. Apparently, titanite started to crystallize and higher T but continued to
726 form at lower T as the enclaves quenched and then slowly cooled (Fig. 18D & 18E).

727 After magmatic crystallization, the resorbed ilmenite in the patchy zones experienced
728 subsolidus oxy-exsolution and further down temperature conversions to rutile, pyrophanite, and
729 brookite (Fig. 18F). At the same time, magmatic phenocrysts of magnetite evolved to become
730 nearly Ti-free, plagioclase became Or-poor, and K-feldspar lost Ab.

731 Eventually, after final solidification of the Little Cottonwood granodiorite, hydrothermal
732 fluids coursed through the stock along fractures and grain boundaries to produce secondary
733 titanite (Fig. 18F). The O-isotopic composition of hydrothermal titanite rims (type 2A) in Little
734 Cottonwood stock suggest that the fluid may have been magmatic initially, with $\delta^{18}O$ in
735 hydrothermal titanite as high 5.2‰—in agreement with John's (1989) interpretation that the
736 hydrothermal fluids were largely magmatic. However, this hydrothermal titanite is
737 compositionally distinct from the magmatic titanite and does not have high Zr-Hf content or
738 calculated temperatures like the hydrothermal titanite in the Notch Peak granite. Moreover, the
739 $\delta^{18}O$ of titanite in chloritized biotite (type 2B) ranges to as low as 1.7‰ indicating an increased

role for meteoric water at lower T. King et al. (2001) found a similar isotopic contrast between green hydrothermal/metamorphic titanite (1.3‰) and igneous titanite (4.6‰) in the Little Cottonwood stock.

During this stage, BSE-dark anhedral extensions (type 2A) grew on existing titanite (Fig. 18F). Type 2A titanite has lower concentrations of HFSE, including REE, and higher F, Mg, U and Al compared to magmatic titanite in the stock. The latter four elements are relatively soluble in fluid, especially U in its 6+ state, and became enriched in the hydrothermal titanite. HFSE concentrations are probably low because of their relatively low solubility in aqueous fluids. High Nb/Ta and Th/U ratios are also the result of hydrothermal alteration, as described above for the Notch Peak titanites. Likewise, HREE are more depleted than LREE in the hydrothermal titanite, because of the higher field strengths of these smaller ions and their lower solubilities. Hydrothermal titanite also lacks negative Eu anomalies suggesting the hydrothermal fluid was more oxidized (magnetite is the major secondary oxide), increasing the proportion of Eu^{3+} and allowing Eu to behave like other REE; consequently, this type of hydrothermal titanite has smooth REE patterns without Eu anomalies. Ti was probably derived from the re-equilibration of titaniferous magnetite to magnetite in the cooling pluton. At lower temperatures, the fluid-driven conversion of biotite (with several percent Ti) to nearly Ti-free chlorite released Ti, Al, and F to form tiny blades of titanite (type 2B) along permeable cleavage traces. This titanite has even lower REE concentrations than type 2A, but higher F and Al concentrations, and strong positive Eu anomalies (Fig. 12). This is evidence that magmatic plagioclase had begun to alter, releasing Ca, Al, and Eu to the fluid for consumption by titanite forming in the biotite (e.g., Abraham et al. 1994). By the time this type of titanite crystallized, any REE in the hydrothermal fluids may have been used up in the formation of type 2A titanite or the solubility of REE was lower in the cooler

763 fluids dominated by meteoric water. Unlike at Notch Peak, no replacement titanite (type 2T) was
764 found, indicating less interaction with oxidized hydrothermal fluids. Low Zr contents in
765 hydrothermal titanite yield temperatures as low as 600°C, but average about 690°C—30 to 40°
766 cooler than for magmatic titanite (Fig. 14).
767

768 ## IMPLICATIONS

769 Titanite is a versatile tool that can be used to understand the magmatic and post-
770 magmatic histories of plutonic rocks. This is due to its slow element diffusion rates,
771 incorporation of a variety of trace elements, stability under magmatic and hydrothermal
772 conditions, and its occurrence in many plutonic rocks (e.g., Aleinikoff et al. 2002; Hayden et al.
773 2008; Bonamici et al. 2011; and Stearns et al. 2020). BSE images and correlative compositional
774 and isotopic variations form a record of crystallization and alteration.
775 We exploited these features to examine the relationship between titanite compositions
776 and growth patterns, during crystallization, cooling, and post-emplacement alteration of calc-
777 alkaline plutons from Utah. Based on this study, titanite textures and compositions can be used to
778 identify distinctive batches of magma (e.g., the differences between Notch Peak and Little
779 Cottonwood titanite) and to decipher magmatic evolution within a plutonic system (e.g.,
780 differences between the aplites and granite at Notch Peak). Titanite can also be an important
781 indicator of magma mixing providing hints about changes in titanite forming reactions, along
782 with the temperature, fO_2, and composition of the different components (e.g., the Little
783 Cottonwood stock and its mafic enclaves).
784 Unlike zircon, titanite typically records evidence for hydrothermal alteration as secondary
785 titanite replaces or crystallizes on the margins of magmatic titanite. Compared to magmatic

titanite, hydrothermal titanite has low Th, Nb, Ta, high Nb/Ta, and low Th/U ratios, low REE content, systematic changes in Eu anomalies, higher U, F, and sometimes Al. Thus, titanite compositions can be used to infer fluid temperature, composition, and oxidation state, as well as alteration processes (i.e., phases involved in reactions that make titanite). Moreover, the BSE textures, trace element, major element (F, Al, and Fe) and O-isotopic composition of secondary titanite can be used to evaluate the origin of various hydrothermal fluids. For example, secondary titanite that formed from magmatic fluids with higher temperature and high $\delta^{18}O$ can be distinguished from titanite that formed at lower temperatures and non-magmatic fluids. This approach should be useful for others attempting to unravel complex magmatic and hydrothermal histories of granitic plutons.

On the other hand, our studies indicate that U-Th-Pb geochronology with titanite is complicated by the ease in which titanite alters and by the mobility of U, which may be 3 to 5 times higher in concentration in hydrothermal titanite compared to coexisting magmatic titanite (Supplement Fig. B15). Fortunately, BSE images and geochemistry can help sort primary from hydrothermal titanite, but laser ablation may encounter small domains of altered titanite that are undetected. Moreover, Al-in-titanite geobarometry (Erdmann et al. 2019) does not look promising. A 0.14 GPa difference (0.17 to 0.31 GPa corresponding to depths of about 6 to 11 km) in crystallization pressure across the Little Cottonwood stock is indicated by structural geology, fluid inclusions, and low temperature thermochronology (e.g., Parry and Bruhn 1987; John 1989; Kowallis et al. 1990; Armstrong et al. 2003; Ehlers et al. 2003). This difference is not detected with Al_2O_3 concentrations in titanite. Instead, calculated pressure and Al_2O_3 concentrations in magmatic titanite are about the same across the pluton (average 0.198 +/- 0.014

GPa and 1.36 +/-0.14 wt.% Al_2O_3). To reproduce the high pressure indicated for the western margin of the pluton, Al_2O_3 contents would need to be nearly double this average (2.47 wt.%).

ACKNOWLEDGEMENTS

We thank Diego Fernandez for help using the University of Utah's LA-ICP-MS, and John Valley and Kouki Kitajima at the University of Wisconsin for use of the WiscSIMS. Tober Dyorich and Levi DeCrescenzo helped with sample preparation and Michael Standing assisted with the scanning electron microscope. Funds were provided by Brigham Young University and the National Science Foundation through equipment grants for the LA-ICP-MS, EMP, and XRF spectrometer.

817 REFRENCES

818 Abraham, A.P.G., Davis, D.W., Kamo, S.L., and Spooner, E.T.C. (1994) Geochronological
819 constraints on late Archean magmatism deformation and gold–quartz vein mineralization in the
820 northwestern Anialik River greenstone belt and igneous complex, Slave Province, NWT.
821 Canadian Journal of Earth Sciences, 31(8), 1365-1383.

822 Aleinikoff, J.N., Wintsch, R.P., Fanning, C.M., and Dorais, M.J. (2002) U-Pb geochronology of
823 zircon and polygenetic titanite from the Glastonbury Complex, Connecticut, USA; an integrated
824 SEM, EMPA, TIMS, and SHRIMP study. Chemical Geology, 188(1-2), 125-147.

825 Angiboust, S. and Harlov, D. (2017) Ilmenite breakdown and rutile-titanite stability in
826 metagranitoids: Natural observations and experimental results. American Mineralogist, 102(8),
827 1696-1708.

828 Armstrong, P.A., Ehlers, T.A., Chapman, D.S., Farley, K.A., and Kamp, P.J. (2003) Exhumation
829 of the central Wasatch Mountains, Utah: 1. Patterns and timing of exhumation deduced from
830 low-temperature thermochronology data. Journal of Geophysical Research: Solid Earth, 108(B3).

831 Bauer, J. (2015) Complex zoning patterns and rare earth element variations across titanite
832 crystals from the Half Dome Granodiorite, Central Sierra Nevada, California, 76 p. M.S. thesis,
833 University of North Carolina, Chapel Hill.

834 Best, M.G., Christiansen, E.H., de Silva, S., and Lipman, P.W. (2016) Slab-rollback ignimbrite
835 flareups in the southern Great Basin and other Cenozoic American arcs: A distinct style of arc
836 volcanism. Geosphere, 12(4), 1097-1135.

837 Boehnke, P., Watson, E.B., Trail, D., Harrison, T.M., and Schmitt, A.K. (2013) Zircon saturation
838 re-revisited. Chemical Geology, 351, 324-334.

839 Bonamici, C.E., Kozdon, R., Ushikubo, T., and Valley, J.W. (2011) High-resolution P-T-t paths
840 from $\delta^{18}O$ zoning in titanite: A snapshot of late-orogenic collapse in the Grenville of New York.
841 Geology, 39(10), 959-962.

842 Bonamici, C.E., Kozdon, R., Ushikubo, T., and Valley, J.W. (2014) Intragrain oxygen isotope
843 zoning in titanite by SIMS: Cooling rates and fluid infiltration along the Carthage-Colton
844 Mylonite Zone, Adirondack Mountains, NY, USA. Journal of Metamorphic Petrology, 32(1), 71-
845 92.

846 Bonamici, C.E., Fanning, C.M., Kozdon, R., Fournelle, J.H., and Valley, J.W. (2015) Combined
847 oxygen-isotope and U-Pb zoning studies of titanite: New criteria for age preservation. Chemical
848 Geology, 398, 70-84.

849 Broska, I., and Petrík, I. (2015) Variscan thrusting in I- and S-type granitic rocks of the Tribeč
850 Mountains, Western Carpathians (Slovakia): evidence from mineral compositions and monazite
851 dating. Geologica Carpathica, 66(6), 455-471.

852 Broska, I., Harlov, D., Tropper, P., and Siman, P. (2007) Formation of magmatic titanite and
853 titanite–ilmenite phase relations during granite alteration in the Tribeč Mountains, Western
854 Carpathians, Slovakia. Lithos, 95(1), 58-71.

855 Bruand, E., Storey, C., Fowler, M., and Heilimo, E. (2019) Oxygen isotopes in titanite and
856 apatite, and their potential for crustal evolution research. Geochimica et Cosmochimica Acta,
857 255, 144-162.

858 Chen, W., Xiong, X., Wang, J., Xue, S., Li, L., Liu, X., Ding, X., and Song, M. (2018) TiO_2
859 solubility and Nb and Ta partitioning in rutile-silica-rich supercritical fluid systems: Implications

860 for subduction zone processes. Journal of Geophysical Research: Solid Earth, 123(6), 4765-
861 4782.

862 Cherniak, D.J. (2010) Diffusion in accessory minerals: zircon, titanite, apatite, monazite and
863 xenotime. Reviews in Mineralogy and Geochemistry, 72(1), 827-869.

864 Christiansen, E.H., Kowallis, B.J., Dorais, M.J., Hart, G.L., Mills, C.N., Pickard, M., and Parks,
865 E. (2015) The record of volcanism in the Brushy Basin Member of the Morrison Formation:
866 Implications for the Late Jurassic of western North America. In Anderson, T.H., Didenko, A.N.,
867 Johnson, C.L., Khanchuk, A.I., and MacDonald, J.H., Jr., Eds., Late Jurassic Margin of
868 Laurasia—A Record of Faulting Accommodating Plate Rotation, Geological Society of America
869 Special Paper 513, 399-439.

870 Christiansen, E.H., and Venchiarutti, D.A. (1990) Magmatic inclusions in rhyolites of the Spor
871 Mountain Formation, western Utah: Limitations on compositional inferences from inclusions in
872 granitic rocks: Journal of Geophysical Research, 95, 17,717-17,728.

873 Colombini, L.L., Miller, C.F., Gualda, G.A.R., Wooden, J.L., and Miller, J.S. (2011) Sphene and
874 zircon in the Highland Range volcanic sequence (Miocene, southern Nevada, USA): elemental
875 partitioning, phase relations, and influence on evolution of silicic magma. Mineralogy and
876 Petrology, 102(1), 29.

877 Constenius, K.N., Clark, D.J., King, J.K., and Ehler, J.B. (2011) Interim geologic map of the
878 Provo 30’ x 60’ quadrangle, Utah, Wasatch, and Salt Lake Counties, Utah. Utah Geological
879 Survey, Open-file report 586DM, scale 1:62.5000.

880 Dailey, S.R., Christiansen, E.H., Dorais, M.J., Kowallis, B.J., Fernandez, D.P., and Johnson,
881 D.M. (2018) Origin of the fluorine- and beryllium-rich rhyolites of the Spor Mountain
882 Formation, Western Utah. American Mineralogist, 103(8), 1228-1252.

883 Deer, W.A., Howie, R.A., Zussman, J. (1982) Rock Forming minerals. Orthosilicates Vol. 1A,
884 Longman, London.

885 Ehlers, T.A., Willett, S.D., Armstrong, P.A., and Chapman, D.S. (2003) Exhumation of the
886 central Wasatch Mountains, Utah: 2. Thermokinematic model of exhumation, erosion, and
887 thermochronometer interpretation. Journal of Geophysical Research: Solid Earth, 108(B3).
888 doi:10.1029/2001JB001723

889 Erdmann, S., Wang, R., Huang, F., Scaillet, B., Zhao, K., Liu, H., Chen, Y., and Faure, M.
890 (2019) Titanite: A potential solidus barometer for granitic magma systems. Comptes Rendus
891 Geoscience, 351(8), 551-561.

892 Frost, B.R., Barnes, C.G., Collins, W.J., Arculus, R.J., Ellis, D.J., and Frost, C.D. (2001a) A
893 geochemical classification for granitic rocks. Journal of Petrology, 42(11), 2033-2048.

894 Frost, B.R., Chamberlain, K.R., and Schumacher, J.C. (2001b) Sphene (titanite); phase relations
895 and role as a geochronometer. Chemical Geology, 172(1-2), 131-148.

896 Garber, J.M., Hacker, B.R., Kylander-Clark, A.R.C., Stearns, M., and Seward, G. (2017)
897 Controls on trace element uptake in metamorphic titanite; implications for petrochronology.
898 Journal of Petrology, 58(6), 1031-1058.

899 Gehman, H.M. (1958) Notch Peak intrusive, Millard County, Utah—Geology, Petrogenesis, and
900 Economic Deposits. Utah Geological and Mineralogical Survey Bulletin 62, 1-50.

901 Hanson, S.L. (1995) Mineralogy, petrology, geochemistry and crystal size distribution of
902 Tertiary plutons of the central Wasatch Mountains, Utah, 384 p. Ph.D. thesis, University of Utah.

903 Hayden, L.A., Watson, E.B., and Wark, D.A. (2008) A thermobarometer for sphene (titanite).
904 Contributions to Mineralogy and Petrology, 155(4), 529-540.

905 Henze, P.K. (2020) Implications of geochemistry and textures of titanite for the geologic
906 histories of the Notch Peak intrusion and Little Cottonwood stock, Utah, 168 p. M.S. thesis,
907 Brigham Young University, Provo, Utah.

908 Hintze, L.F. (1974) Geology of the Notch Peak 15' quadrangle. U.S. Geological Survey Open
909 File Map 636, scale 1/24,000.

910 Hintze, L.F., and Davis, F.D. (2002) Geologic Map of the Tule Valley 30’ x 60’ Quadrangle and
911 parts of the Ely Fish Springs, and Kern Mountains 30’ x 60’ Quadrangles, Northwest Millard
912 County, Utah. Utah Geological Survey, scale 1:100,000.

913 Hintze, L.F., and Kowallis, B.J. (2021) Geologic History of Utah, 266 p. Department of
914 Geological Sciences, Brigham Young University, Provo, Utah.

915 Jensen, C.G., Christiansen, E.H., and Keith, J.D. (2022) Multi-stage construction of the Little
916 Cottonwood stock, Utah: Origin, intrusion, venting, mineralization, and mass movement,
917 Geosphere, in press.

918 Jiang, P., Yang, K.-F., Fan, H.-R., Liu, X., Cai, Y.-C., and Yang, Y.-H. (2016) Titanite-scale
919 insights into multi-stage magma mixing in Early Cretaceous of NW Jiaodong terrane, North
920 China Craton. Lithos, 258-259, 197-214.

John, D.A. (1989) Geologic setting, depths of emplacement, and regional distribution of fluid inclusions in intrusions of the central Wasatch Mountains, Utah. Economic Geology, 84(2), 386-409.

Kelly, J.L., Fu, B., Kita, N.T., and Valley, J.W. (2007) Optically continuous silcrete quartz cements of the St. Peter Sandstone: High precision oxygen isotope analysis by ion microprobe. Geochimica et Cosmochimica Acta, 71(15), 3812-3832.

King, E.M., Valley, J.W., Davis, D.W., and Kowallis, B.J. (2001) Empirical determination of oxygen isotope fractionation factors for titanite with respect to zircon and quartz. Geochimica et Cosmochimica Acta, 65(18), 3165-3175.

Kita, N.T., Ushikubo, T., Fu, B., and Valley, J.W. (2009) High precision SIMS oxygen isotope analysis and the effect of sample topography. Chemical Geology, 264(1), 43-57.

Kohn, M.J. (2017) Titanite petrochronology. Reviews in Mineralogy and Geochemistry, 83, 419-441.

Kontonikas-Charos, A., Ehrig, K., Cook, N.J., and Ciobanu, C.L. (2019) Crystal chemistry of titanite from the Roxby Downs Granite, South Australia: insights into petrogenesis, subsolidus evolution and hydrothermal alteration. Contributions to Mineralogy and Petrology, 174, 59. https://doi.org/10.1007/s00410-019-1594-2

Kowallis, B.J., Christiansen, E.H., Dorais, M.J., Winkel, A., Henze, P., Franzen, L., Webb, H. (2018) Compositional variation of Fe, Al, and F in titanite (sphene). Geological Society of America Abstracts with Programs, 50 (6) ISSN 0016-7592, doi: 10.1130/abs/2018AM-320564.

941 Kowallis, B.J., Ferguson, J., and Jorgensen, G.J. (1990) Uplift along the Salt Lake segment of
942 the Wasatch fault from apatite and zircon fission track dating in the little Cottonwood stock.
943 International Journal of Radiation Applications and Instrumentation. Part D. Nuclear Tracks and
944 Radiation Measurements, 17(3), 325-329.

945 Kubeš, M., Leichmann, J., Wertich, V., Mozola, J., Holá, M., Kanický, V. and Škoda, R. (2021)
946 Metamictization and fluid-driven alteration triggering massive HFSE and REE mobilization from
947 zircon and titanite: Direct evidence from EMPA imaging and LA-ICP-MS analyses. Chemical
948 Geology, 58, 120593.

949 Lackey, J.S., Valley, J.W., Chen, J.H., and Stockli, D.F. (2008) Dynamic magma systems,
950 crustal recycling, and alteration in the central Sierra Nevada batholith: The oxygen isotope
951 record. Journal of Petrology, 49(7), 1397-1426.

952 Laurent, O., Zeh, A., Gerdes, A., Villaros, A., Gros, K., and Slaby, E. (2017) How do granitoid
953 magmas mix with each other? Insights from textures, trace element and Sr-Nd isotopic
954 composition of apatite and titanite from the Matok Pluton (South Africa). Contributions to
955 Mineralogy and Petrology, 172(9).

956 Lee, D.E., and Christiansen, E.H. (1983) The granite problem as exposed in the southern Snake
957 Range, Nevada. Contributions to Mineralogy and Petrology, 83(1), 99-116.

958 Lee, D.E., Stacey, J.S.D., and Fisher, L. (1986) Muscovite phenocrystic two-mica granites of NE
959 Nevada are Late Cretaceous in age, In Shorter Contributions to Isotope Research: U.S.
960 Geological Survey Bulletin 1622, 31–39.

961 Liu, Y., Fan, Y., Zhou, T., Zhang, L., White, N.C., Hong, H. and Zhang, W. (2018) LA-ICP-MS
962 titanite U-Pb dating and mineral chemistry of the Luohe magnetite-apatite (MA)-type deposit in
963 the Lu-Zong volcanic basin, Eastern China. Ore Geology Reviews, 92, 284-296.

964 Marsh, A.J., and Smith, R.K. (1997) The Oligocene Little Cottonwood Stock, central Wasatch
965 Mountains, Utah; an example of compositional zoning by side-wall fractional crystallization of
966 an arc-related intrusion. The Mountain Geologist, 34(3), 83-95.

967 Maughan, L.L., Christiansen, E.H., Best, M.G., Gromme, C.S., Deino, A.L. and Tingey, D.G.,
968 (2002) The Oligocene Lund Tuff, Great Basin, USA: a very large volume monotonous
969 intermediate. Journal of Volcanology and Geothermal Research, 113(1-2), 129-157.

970 Mazdab, F.K., Johnson, D.A., and Barton, D.B. (2008) Trace element characteristics of
971 hydrothermal titanite from iron-oxide-Cu-Au (IOCG) mineralization. Geochimica
972 Cosmochimica Acta, 72(12), A609.

973 McDonough, W.F., and Sun, S.S. (1995) The composition of the Earth. Chemical Geology,
974 120(3), 223-253.

975 McKean, A.P., and Solomon B.J. (2018) Interim Geologic Map of the Draper Quadrangle, Salt
976 Lake and Utah Counties, Utah, Utah Geological Survey, scale 1:24,000.

977 McLeod, G.W., Dempster, T.J., and Faithfull, J.W. (2011) Deciphering magma-mixing processes
978 using zoned titanite from the Ross of Mull Granite, Scotland. Journal of Petrology, 52(1), 55-82.

979 Melnik, O. E., and Bindeman, I. N. (2018) Modeling of trace elemental zoning patterns in
980 accessory minerals with emphasis on the origin of micrometer-scale oscillatory zoning in zircon:
981 American Mineralogist, 103, 355-368.

982 Middlemost, E.A., (2013) Magmas, Rocks and Planetary Development. 299 p. New York,
983 Routledge.

984 Middleton, A.W., Förster, H.-J., Uysal, I.T., Golding, S.D., and Rhede, D. (2013) Accessory
985 phases from the Soultz monzogranite, Soultz-sous-Forêts, France: Implications for titanite
986 destabilisation and differential REE, Y and Th mobility in hydrothermal systems. Chemical
987 Geology, 335, 105-117.

988 Miyashiro, A. (1978) Nature of alkalic volcanic rock series. Contributions to Mineralogy and
989 Petrology, 66(1), 91-104.

990 Morad, S., Sirat, M., El-Ghali, M.A.K., and Mansurbeg, H. (2011) chloritization in Proterozoic
991 granite from the Aspo Laboratory, southeastern Sweden; record of hydrothermal alterations and
992 implications for nuclear waste storage. Clay Minerals, 46(3), 495-513.

993 Nabelek, P.I., O'Neil, J.R., and Papike, J.J. (1983) Vapor phase exsolution as a controlling factor
994 in hydrogen isotope variation in granitic rocks: The Notch Peak granitic stock, Utah. Earth and
995 Planetary Science Letters, 66, 137-150.

996 Nabelek, P.I. (1986) Trace-element modeling of the petrogenesis of granophyres and aplites in
997 the Notch Peak granitic stock, Utah. American Mineralogist, 71(3-4), 460-471.

998 Nabelek, P.I., Papike, J.J., and Laul, J.C. (1986) The Notch Peak granitic stock, Utah; origin of
999 reverse zoning and petrogenesis. Journal of Petrology, 27(5), 1035-1069.

1000 Nabelek, P.I., Hanson, G.N., Labotka, T.C., and Papike, J.J. (1988) Effects of fluids on the
1001 interaction of granites with limestones: The Notch Peak stock, Utah. Contributions to
1002 Mineralogy and Petrology, 99(1), 49-61.

1003 Nabelek, P.I., and Labotka, T.C. (1993) Implications of geochemical fronts in the Notch Peak
1004 contact-metamorphic aureole, Utah, USA. Earth and Planetary Science Letters, 119(4), 539-559.

1005 Nakada, S. (1991) Magmatic processes in titanite-bearing dacites, central Andes of Chile and
1006 Bolivia. American Mineralogist, 76(3-4), 548-560.

1007 Norman, M.D., Pearson, N.J., Sharma, A., and Griffin, W.L. (1996) Quantitative analysis of
1008 trace elements in geological materials by laser ablation ICPMS: instrumental operating
1009 conditions and calibration values of NIST glasses. Geostandards & Geoanalytical Research,
1010 20(2), 247-261.

1011 Novick, J.S., and Labotka, T.C. (1990) Metamorphic fluids in the Notch Peak contact-
1012 metamorphic aureole; evidence from fluid inclusions. American Mineralogist, 75(3-4), 387-391.

1013 Pan, L.-C., Hu, R.-Z., Bi, X.-W., Li, C., Wang, X.-S., and Zhu, J.-J. (2018) Titanite major and
1014 trace element compositions as petrogenetic and metallogenic indicators of Mo ore deposits:
1015 Examples from four granite plutons in the southern Yidun arc, SW China. American
1016 Mineralogist, 103(9), 1417-1434.

1017 Parry, W.T., and Bruhn, R.L. (1987) Fluid inclusion evidence for minimum 11 km vertical offset
1018 on the Wasatch fault, Utah. Geology, 15(1), 67-70.

1019 Paterson, B.A., Stephens, W.E., and Herd, D.A. (1989) Zoning in granitoid accessory minerals as
1020 revealed by backscattered electron imagery. Mineralogical Magazine, 53, Part 1(369), 55-61.

1021 Paterson, B.A., and Stephens, W.E. (1992) Kinetically induced compositional zoning in titanite;
1022 implications for accessory-phase/melt partitioning of trace elements. Contributions to
1023 Mineralogy and Petrology, 109(3), 373-385.

1024 Paton, C., Hellstrom, J., Paul, B., Woodhead, J., and Hergt, J. (2011) Iolite: Freeware for the
1025 visualisation and processing of mass spectrometric data. Journal of Analytical Atomic
1026 Spectrometry, 26, 2508–2518.

1027 Piccoli, P., Candela, P., and Rivers, M. (2000) Interpreting magmatic processes from accessory
1028 phases; titanite, a small-scale recorder of large-scale processes. Transactions of the Royal
1029 Society of Edinburgh: Earth Sciences, 91, Parts 1-2, 257-267.

1030 Pearce, J.A., Harris, N.B.W., and Tindle, A.G. (1984) Trace element discrimination diagrams for
1031 the tectonic interpretation of granitic rocks. Journal of Petrology, 25(4), 956-983.

1032 Rossetti, F., Asti, R., Faccenna, C., Gerded, A., Lucci, F., and Theye, T. (2017) Magmatism and
1033 crustal extension: Constraining activation of the ductile shearing along the Gediz detachment,
1034 Menderes Massif. Lithos, 282-283, 145-162.

1035 Shore, M., and Fowler, A.D. (1996) Oscillatory zoning in minerals; a common phenomenon. The
1036 Canadian Mineralogist, 34(6), 1111-1126.

1037 Smyk, E., Hollings, P., Baker, M., Cooke, D.R., Thompson, J.A., Thompson, J.M., and Creaser,
1038 R. (2018) Geochemistry and geochronology of the intrusive rocks of the central Wasatch
1039 Mountains igneous belt, Utah, USA: implications for porphyry mineralization. Utah Geological
1040 Association Publication, 47, 305-327.

1041 Spandler, C., Hammerli, J., Sha, P., Hilbert-Wolf, H., Hu, Y., Roberts, E., and Schmitz, M.
1042 (2016) MKED1: A new titanite standard for in situ analysis of Sm–Nd isotopes and U–Pb
1043 geochronology. Chemical Geology, 425, 110-126.

1044 Speer, J.A., and Gibbs, G.V. (1976) The crystal structure of synthetic titanite, $CaTiOSiO_4$, and
1045 the domain textures of natural titanites. American Mineralogist, 61, 238-247.

1046 Stearns, M.A., Bartley, J.M., Bowman, J.R., Forster, C.W., Beno, C.J., Riddle, D.D., Callis, S.J.,
1047 Udy, N.D. (2020) Simultaneous magmatic and hydrothermal regimes in Alta–Little Cottonwood
1048 Stocks, Utah, USA, recorded using multiphase U-Pb petrochronology. Geosciences, 10, 129.

1049 Uher, P., Broska, I., Krzemińska, E., Ondrejka, M., Mikuš, T., and Vaculovič, T. (2019) Titanite
1050 composition and SHRIMP U–Pb dating as indicators of post-magmatic tectono-thermal activity:
1051 Variscan I-type tonalites to granodiorites, the Western Carpathians. Geologica Carpathica, 70(6),
1052 449-470.

1053 Vogel, T.A., Cambray, F.W., and Constenius, K.N. (2001) Origin and emplacement of igneous
1054 rocks in the central Wasatch Mountains, Utah. Rocky Mountain Geology, 36(2), 119-162.

1055 Wolff, J.A. and Storey, M., (1984) Zoning in highly alkaline magma bodies. Geological
1056 Magazine, 121(6), 563-575.

1057 Wones, D.R. (1989) Significance of the assemblage titanite + magnetite + quartz in granitic
1058 rocks. American Mineralogist, 74(7-8), 744-749.

1059 Xie, L., Wang, R.C., Chen, J., and Zhu, J.C. (2010) Mineralogical evidence for magmatic and
1060 hydrothermal processes in the Qitianling oxidized tin-bearing granite (Hunan, South China):
1061 EMP and (MC)-LA-ICPMS investigations of three types of titanite. Chemical Geology, 276(1-
1062 2), 53-68.

1063 Xirouchakis, D., Lindsley, D.H., and Frost, B.R. (2001) Assemblages with titanite ($CaTiOSiO_4$),
1064 Ca-Mg-Fe olivine and pyroxenes, Fe-Mg-Ti oxides, and quartz: Part II. Application. American
1065 Mineralogist, 86(3), 254-264.

1066 Yonkee, W.A., and Weil, A.B. (2015) Tectonic evolution of the Sevier and Laramide belts
1067 within the North American Cordillera orogenic system. Earth-Science Reviews, 150, 531-593.

1068 Zhang, X.Y., Cherniak, D.J., and Watson, E.B. (2006) Oxygen diffusion in titanite: Lattice
1069 diffusion and fast-path diffusion in single crystals. Chemical Geology, 235 (1-2), 105-123.

1070 Zhao, Z., Wang, C.Y., Wei, B., and Dou, J. (2021) Elemental and Nd isotopic compositions of
1071 zoned titanite in mafic microgranular enclaves of the Early Cretaceous Sanguliu granitic pluton
1072 in the North China Craton: Insights into magma mixing process. Lithos, 392-393, 106138,
1073 https://doi.org/10.1016/j.lithos.2021.106138.

1074

FIGURE CAPTIONS

Figure 1. Geologic maps of the (A) Little Cottonwood and (B) Notch Peak plutons, Utah, with sample locations. Altered samples are represented by unfilled circles. Titanite was analyzed for its oxygen isotopic composition in samples marked with diagonal slashes. Map for the Little Cottonwood area is modified from Constenius et al. (2011) and Jensen et al. (2022); the Notch Peak map is modified from Hintze (1974), Hintze and Davis (2002), and Nabelek et al. (1986).

Figure 2. Whole-rock compositions of the plutonic rocks. (A) Total alkali-silica diagram (Middlemost, 2013). (B) Modified alkali-lime index (Frost et al. 2001a). (C) Low FeO/(FeO+MgO) ratios indicate the oxidized character of the magmas (Miyashiro 1978). (D) Trace element concentrations of are consistent with a subduction origin for the plutons (Pearce et al. 1984). (E) Chondrite-normalized REE patterns. Monzodioritic Little Cottonwood enclaves are much more enriched in REE than the granitic host rocks. (F) Mantle-normalized trace element patterns. Chondrite and primitive mantle values taken from McDonough and Sun (1995). Hydrothermally altered samples have symbols with white borders (A-D) or as dashed line (E and F).

Figure 3. Titanite compositions correlate with the textural types as shown by this grain (LC-SB-4) from the Little Cottonwood stock. (A) BSE image with color coded spots for EMP and black circles for LA-ICP-MS analyses. Yellow arrows point to some dissolution surfaces. (B) Textural map of the grain showing several periods of magmatic and post-magmatic growth. (C) F concentrations increase and REE concentrations decrease from core (red) to rim (cyan), especially in secondary titanite (2A and 2B). The green field shows the range of all data from the Little Cottonwood stock. (D) Fe and Al concentrations largely overlap for the different types.

Titanite replacing biotite (type 2B, purple), however, has low Fe/Al ratios. (E) REE concentrations are low in the outermost oscillatory zones(green 1O2) and in the secondary non-magmatic titanite (cyan 2A and purple 2B). Secondary types also lack negative Eu anomalies.

Figure 4. Titanite compositions and textural types for Notch Peak grain (NP-6-4). (A) BSE image and analytical spots—EMPA (colored coded by type of zoning) was followed by LA analysis (black circles). Yellow arrows point to dissolution surfaces. (B) Textural map of the grain reveals two periods of oscillatory growth (1O1 and 1O2) and two types of secondary hydrothermal titanite (2T1 and 2T2). (C) F concentrations increase and REE concentrations decrease from core to rim and are especially low in the secondary zones (2T blue and purple).The green fields include all the data from the Notch Peak granite. (D) Fe and Al concentrations overlap for the different types, but Fe/Al ratios are higher in the secondary hydrothermal titanite (cyan and purple), and Al extends to lower values for the secondary types. (E) REE patterns. Yellow and red zones are primary magmatic titanite and have high REE concentrations, lower La/Yb ratios, middle REE enrichment and negative Eu anomalies. Hydrothermal titanite (purple and cyan) lacks the middle REE enrichment of typical magmatic titanite and lacks negative Eu anomalies in 3 of the 4 analyses.

Figure 5. Titanite (HFT-18-2-11) in a mafic enclave from the Little Cottonwood stock. (A) BSE image with color-coded EMP analytical spots and black circles for LA-ICP-MS analyses. Yellow arrows point to dissolution surfaces. An irregular core is surrounded by patchy mantle (1Pm). This type of texture is only found in the enclaves. (B) Textural map of the grain showing different periods of magmatic growth. (C) All the primary types in the grain have similar F and REE concentrations without the typical changes toward rim. Green field shows range of all the

data from enclaves in the pluton. (D) Fe and Al similarly overlap. (E) REE patterns are typical for magmatic titanite except there are portions of the grain that lack Eu anomalies.

Figure 6. In BSE images, patchy cores (1Pc) in titanite have alternating dark and bright zones with highly irregular shapes, gradational to sharp wavy boundaries, and resorbed inclusions of ilmenite (A; grain LC-HFT-1). The greater magnification in (B) shows the details of this mottled texture. The ilmenite inclusions have experienced subsolidus oxy-exsolution and now consist of ilmenite, brookite, and magnetite. These patchy cores are prominent in titanite from the Little Cottonwood stock but are uncommon in Notch Peak granite. (C) BSE image of area in yellow box in B. (D) Maps of Ti, Fe, and Mn for grain in C. Magmatic high-Fe ilmenite inclusions experienced oxy-exsolution to form ilmenite (Ilm - pink on the Mn map and light gray on BSE image), low-Ti magnetite (Mag - dark red on the Fe map and white on BSE image), and brookite (Brk, dark blue in Ti and white on Fe maps and dark gray on BSE image) in the slowly cooled pluton.

Figure 7. Titanite replaced (3R) by secondary minerals in the Notch Peak pluton. (A) Grain NP-005-6 has been completely replaced by secondary ilmenite, brookite, magnetite, biotite, monazite, xenotime, Nb-Ti oxides, Ca-REE-fluorides, and quartz, but retains the original shape of the crystal. (B) Grain NP-002-5 is partially replaced. Unzoned (1U), oscillatory (1O), and bright sectors (1S) are also present.

Figure 8. Composition of titanite from the Notch Peak pluton. A) REE patterns of different titanite zones reveal the depletion of REE in secondary hydrothermal titanite (type 2). B) The composition of average hydrothermal titanite divided by average magmatic titanite (LA-ICPMS data except for F, Fe, and Al which are from EMPA).

Figure 9. F versus LREE (by EMPA) in (A) Little Cottonwood stock and (B) Notch Peak pluton. According to t-tests, the means are significantly different except for LC-SL and LC-TQ and NP-2 and NP-5.

Figure 10. Average compositions (by EMPA) of titanite in the different units studied. (A) Mn vs. Ti, (B) Y vs. F, (C) La vs. Ce, (D) LREE vs. Fe/Al ratio, and (E) Al vs Fe. On (D), the high-Fe titanite type (2F) from the aplites is not plotted because the Fe/Al ratio (>2.0) is too high. Likewise, type 2B (formed by biotite replacement) is not plotted on (A), (B), and (E) because of its high F and Al and low Ti concentrations. Secondary titanite (2T) in the Little Cottonwood stock averages 0.07 F pfu, while type 2B averages 0.19 F pfu. Ti concentrations are low in type 2B (~0.75 pfu) because of very high Al (~0.20 pfu).

Figure 11. Primitive-mantle normalized plots of average titanite compositions. (A) Primary titanite from Notch Peak has higher concentrations of most plotted elements than that from Little Cottonwood stock, but titanite from Notch Peak aplites has distinctly lower concentrations of REE. Comparison of magmatic and hydrothermal titanite: (B) Notch Peak; (C) Little Cottonwood stock; and (D) Little Cottonwood enclaves. Compared to magmatic titanite, hydrothermal titanite is generally depleted in all these elements, except U and F.

Figure 12. Chondrite-normalized REE plots for different types of titanite in the Little Cottonwood stock. (A) REE patterns for titanite in granodiorite. Bright sectors (1S) unzoned (1U), oscillatory (1O), and patchy core (1Pc) types have similar REE patterns, although the patchy cores tend to have smaller Eu anomalies. Secondary hydrothermal titanite has lower REE contents and lacks Eu anomalies, except for type 2B which has strong positive Eu anomalies. Some patchy zones also have strong positive Eu anomalies (1Pe) that may be evidence for a

secondary origin. (B) REE patterns for titanite from enclaves in the Little Cottonwood stock. Plots for individual analyses are in Supplement B.

Figure 13. Comparisons of magmatic and hydrothermal titanite in the Little Cottonwood stock. (A) Ratio of composition of average secondary to primary titanite in granodiorite. Secondary titanite (2A) is enriched in U, Mg, F, and Al and has low middle REE (Nd to Er), and anomalous Eu compared to primary titanite. (B) Ratio of the composition of average secondary titanite to primary titanite in the mafic enclaves. Secondary titanite (2A) is enriched in U and F and has anomalous Eu compared to primary titanite.

Figure 14. Zr-in-titanite temperatures. Temperature vs. (A) total REE and (B) Eu/Eu*. Compared to primary magmatic titanite (circles), hydrothermal titanite (x) in the Little Cottonwood stock yields lower calculated T (<700°C) and positive Eu anomalies (Eu/Eu* >1). Eu was not as mobile during precipitation of secondary titanite in the Notch Peak intrusion based on the overlap of Eu/Eu* for the two types. In the Little Cottonwood stock, secondary titanite associated or intergrown with biotite (type 2B) has the highest Eu/Eu*, while at Notch Peak the high Fe zones in titanite from the aplites have the highest Eu/Eu*. Zr-in-titanite temperatures were calculated using 0.75 as the $a\mathrm{TiO_2}$.

Figure 15. BSE images of two titanite grains (oNP-1 and oHFT-7) showing $\delta^{18}O$ and Zr-in-titanite temperatures (except for the 2B zone on HFT-7 that was too small to analyze by LA-ICP-MS). In Notch Peak, magmatic (1S,1U, and 1O) and hydrothermal types (2A) have similar $\delta^{18}O$ values. In the Little Cottonwood stock (oHFT-7) $\delta^{18}O$ for titanite associated with biotite (2B) is lower (to 2.3‰) suggesting interaction with meteoric water with low $\delta^{18}O$.

Figure 16. Histograms of $\delta^{18}O$ values in titanite collected using SIMS. $\delta^{18}O$ values for primary titanite from the Notch Peak pluton are typically higher than for titanite from the Little Cottonwood stock (6.0‰ vs. 4.9‰), reflecting the original magmatic compositions. $\delta^{18}O$ of secondary titanite (2A) in the Notch Peak pluton extends to slightly higher values than for primary titanite, while secondary titanite in the Little Cottonwood stocks tends to have lower $\delta^{18}O$, especially in titanite replacing biotite (2B).

Figure 17. Crystallization of titanite in the Notch Peak granite. (A) Unzoned titanite (1U) crystallized from granitic magma. (B) Sporadic dissolution events resorbed part of this grain. (C) New growth of magmatic titanite mantled the unzoned core, usually with oscillations (1O) linked to sector zones (1S). (D) At a later stage, secondary titanite (2A) crystallized from exsolved magmatic fluid to form BSE dark (REE-Y-poor, F-rich) anhedral overgrowths. (E) Some grains were partially replaced by BSE-dark secondary titanite (2T). (F) Locally, titanite was completely replaced by secondary minerals (3R), including ilmenite (blue), magnetite (green), biotite (brown) and a TiO_2 phase (red), during reaction with oxidized fluid.

Figure 18. A typical crystallization path for titanite in the Little Cottonwood stock. (A) Ilmenite (blue) grew in low fO_2, monzondioritic magma. (B) Ilmenite was resorbed when this magma mixed with higher fO_2 calc-alkaline felsic magma. (C) Patchy titanite (1P browns) grew during the reaction of ilmenite with the felsic magma and preserved partially resorbed ilmenite. (D) After mixing, unzoned titanite (1U) mantled the core. (E) Oscillatory growth (1O) ensued to form the rim of the grain. Growth and dissolution alternated. (F) Secondary titanite formed as BSE-dark anhedral overgrowths (2A) or F-rich REE-poor blade-like anhedra (2B) where biotite reacted with fluid to stabilize chlorite.

This is the peer-reviewed, final accepted version for American Mineralogist, published by the Mineralogical Society of America.
The published version is subject to change. Cite as Authors (Year) Title. American Mineralogist, in press.
DOI: https://doi.org/10.2138/am-2022-8241. http://www.minsocam.org/

Table 1. Textural classification of titanite

Symbol	Name	Characteristics	Figure
1U	Unzoned	Lacks systematic zoning	4, 5, 8, 17B
1O	Oscillatory	Oscillatory zones commonly around 1C,1N, or 1Pc	3, 4, 5, 6, 8, 17A
1S	Sector	BSE-bright sector zones formed in conjunction with 1O enriched in HFSE	3, 8, 17A, 17B
1Pc	Patchy core	Mottled core texture with BSE-dark and bright patches, always includes resorbed ilmenite	3, 6, 17B
1Pm	Patchy mantle	Similar to patchy core, but mantles either 1C,1U, or 1Pc	5, Supplement A65
2A	Anhedral	Zoneless titanite, usually BSE-dark, which extends between and into surrounding minerals	3, 17B
2B	Biotite replacement	BSE-dark, anhedral titanite that replaces chloritized biotite	3, 17B
2F	Fe-rich secondary	BSE-bright late overgrowth	Supplement A22, A23
2T	Titanite replacement	Dark titanite with irregular zoning that truncates existing titanite zones	4, 17A
3R	Replaced	Complete replacement of titanite by mixture of silicates, oxides, fluorides, and carbonates	8, Supplement A11

Table 2. Composition of selected titanite grains from the Notch Peak and Little Cottonwood stocks

Grain	Texture	Si (pfu)	Al (pfu)	Ti (pfu)	Fe (pfu)	Ca (pfu)	Mn (pfu)	Nb (pfu)	Tot REE (pfu)	F (pfu)
Notch Peak										
NP-2-1j	1S	0.989	0.064	0.817	0.0650	0.965	0.0064	0.0572	0.0228	0.041
NP-3-2m	1Pc	0.991	0.048	0.893	0.0601	0.971	0.0035	0.0097	0.0175	0.046
NP-2-2d	1O	0.995	0.054	0.873	0.0558	0.975	0.0022	0.0141	0.0234	0.053
NP-5-01a	1O	0.993	0.057	0.874	0.0544	0.979	0.0036	0.0137	0.0187	0.064
oNP-6-3-e	2T	0.986	0.058	0.884	0.0576	1.004	0.0040	0.0004	0.0058	0.089
NP-6-1m	2T	1.022	0.054	0.872	0.0531	0.987	0.0028	0.0014	0.0034	0.097
NP-18-2a-015-e	2F	0.098	0.060	0.826	0.1006	1.028	0.0022		0.0078	0.122
Little Cottonwood										
LC-HFT-4-x	1Pc	0.996	0.064	0.872	0.0581	0.969	0.0008	0.0047	0.0287	0.062
LC-TQ-3-ab	1S	0.982	0.050	0.884	0.0480	0.966	0.0030	0.0270	0.0310	0.027
LC-TQ-4-b	1O	0.994	0.050	0.889	0.0431	0.981	0.0030	0.0099	0.0216	0.052
LC-SB-1-q	1Pc	0.998	0.050	0.899	0.0460	0.960	0.0010	0.0050	0.0330	0.034
LC-SB-4-ae	2A	1.004	0.054	0.895	0.0470	0.991	0.0030	0.0020	0.0034	0.067
oLC-HFT-6d	2B	0.996	0.310	0.647	0.0310	1.010	0.0010	0.0000	0.0020	0.278
Little Cottonwood Mafic Enclaves										
LC-HFT-18-1-11-h	1U	0.996	0.046	0.911	0.0433	0.973	0.0024	0.0056	0.0199	0.034
LC-SB-18-4-3-h	1Pc	0.994	0.046	0.907	0.0380	0.990	0.0020	0.0060	0.0140	0.051
LC-SB-18-4-6-j	1S	0.958	0.068	0.860	0.1290	0.917	0.0060	0.0070	0.0420	0.039
LC-SB-18-4-3-n	1O	0.991	0.046	0.895	0.0512	0.991	0.0034	0.0050	0.0164	0.058
LC-HFT-18-2-11-ad	2A	0.992	0.051	0.904	0.0480	0.990	0.0026	0.0018	0.0090	0.071

*Recalculated based on 3 cations

Table 3. Trace element concentrations in selected titanite grains from Notch Peak and Little Cottonwood stocks

Grain	Textures	V	Y	Zr	Nb	Mo	La	Ce	Pr	Nd	Sm	Eu	Gd	Dy	Ho	Er	Yb	Lu	Hf	W	Pb	Th	U
Notch Peak																							
nb-176-3a	1U	626	2884	561	3143	32	2104	8923	1442	7552	1598	266	1268	804	137	364	272	31	26	1	12	622	120
oNP-1-2a	1S	334	1970	1490	13600	29	2690	8250	1127	4580	798	105	512	349	66	189	223	38	69	127	24	620	1305
NP-6-1d	1O	674	3372	551	3982	32	2356	8925	1515	7681	1720	261	1050	774	127	357	306	37	31	-	10	621	131
NP-6-9a	2T	1350	646	443	2580	30	1870	5900	655	2270	288	53	169	85	21	53	85	13	26	1	8	293	266
NP-6-4d	2T	801	403	638	4141	115	1428	3535	359	1292	191	53	116	63	11	32	41	6	38	-	11	437	609
Notch Peak Aplite																							
NP-18-2a-6a	1U	570	913	748	4059	19	1225	4055	493	1892	221	25	176	133	28	101	135	18	95	7	7	123	122
NP-18-2a-22d	2T	83	131	157	3279	5	365	1027	107	399	44	9	32	23	5	17	20	3	9	2	18	79	217
NP-18-2a-15e	2F	869	1518	298	9961	20	356	1598	285	1449	345	74	298	254	52	159	197	26	51	6	8	54	105
Little Cottonwood																							
LC-SB-5e	1Pc	566	1582	389	1453	71	1907	7625	1113	5371	979	206	668	395	62	135	107	13	22	-	3	314	88
LC-HFT-3a	1Pc	790	879	524	898	33	2350	8800	1060	3420	468	160	264	147	26	84	72	10	35	-	-	251	72
LC-SL-6c	1S	647	2424	717	4226	31	2510	9727	1565	8011	1490	233	1097	688	118	299	211	24	54	2	7	565	102
LC-TQ1b	1O	640	1916	329	2496	31	1084	4510	742	3605	731	144	548	396	68	182	185	24	27	-	6	384	122
LC-SB-4o	2A	658	231	214	490	56	972	2379	255	940	104	31	77	41	7	24	21	4	21	-	13	211	218
oLC-HFT-6a	2B	696	181	130	710	22	403	1210	108	420	56	36	37	25	4	15	18	3	15	6	3	51	214
Little Cottonwood mafic enclaves																							
LC-HFT-18-2-24f	1U	1120	1180	348	1780	78	1910	7680	1060	4130	840	174	387	268	50	95	101	8	27	-	0	351	86
oLC-HFT-18-6-5a	1Up	722	1165	606	1216	35	3010	8020	935	2970	415	127	299	218	40	111	101	14	53	4	3	545	88
oLC-SB-18-5-3e	2T	819	455	467	729	41	1620	3920	355	1310	220	127	134	71	13	35	39	6	19	6	2	331	84
LC-HFT-18-2-23c	1Pm	880	761	486	1440	87	1850	8170	1230	4920	821	279	438	222	31	69	54	4	29	-	-	281	115
LC-HFT-18-2-13b	2A	790	633	281	1190	29	1400	5190	590	2270	299	82	226	123	23	47	59	3	24	-	4	349	500
Uncertainty		683	94	61	177	12	98	323	34	158	38	7	28	305	4	9	10	16	5	1	2	20	11

Concentrations in ppm
- = not detected

This is the peer-reviewed, final accepted version for American Mineralogist, published by the Mineralogical Society of America.
The published version is subject to change. Cite as Authors (Year) Title. American Mineralogist, in press.
DOI: https://doi.org/10.2138/am-2022-8241. http://www.minsocam.org/

Table 4. Average composition of titanite from the Notch Peak and Little Cottonwood stocks

Pluton	Si (pfu)	Al (pfu)	Ti (pfu)	Fe (pfu)
Notch Peak primary	0.994 ± 0.009	0.053 ± 0.009	0.876 ± 0.022	0.055 ± 0.011
Notch Peak secondary	0.995 ± 0.011	0.050 ± .011	0.887 ±0.023	0.053 ± 0.014
Little Cottonwood w/ patchy cores	0.999 ± 0.008	0.049 ± 0.007	0.903 ± 0.014	0.043 ± 0.009
Little Cottonwood w/o patchy cores	0.997 ± 0.010	0.052 ± 0.006	0.893 ± 0.012	0.044 ± 0.007
Little Cottonwood secondary	0.998 ± 0.010	0.057 ± .007	0..886 ± 0.007	0.044 ± 0.007
Little Cottonwood mafic enclaves	0.992 ± 0.037	0.049 ± 0.008	0.902 ± 0.043	0.045 ± 0.009

Composition given in atoms per formula unit (pfu)

*± = 1 standard deviation

This is the peer-reviewed, final accepted version for American Mineralogist, published by the Mineralogical Society of America.
The published version is subject to change. Cite as Authors (Year) Title. American Mineralogist, in press.
DOI: https://doi.org/10.2138/am-2022-8241. http://www.minsocam.org/

Ca (pfu)	Mn (pfu)	Nb (pfu)	Tot REE (pfu)	F (pfu)
0.979 ± 0.018	0.004 ± 0.002	0.012 ± 0.012	0.020 ± 0.007	0.057 ± 0.013
0.990 ± 0.014	0.003 ± 0.001	0.007 ± 0.008	0.012 ± 0.007	0.070 ± 0.017
0.973 ± 0.013	0.002 ± 0.001	0.005 ± 0.002	0.022 ± 0.009	0.046 ± 0.010
0.977 ± 0.014	0.003 ± 0.008	0.008 ± 0.005	0.019 ± 0.009	0.049 ± 0.011
0.988 ± 0.012	0.003 ± 0.001	0.007 ± 0.001	0.011 ± 0.006	0.064 ± 0.009
0.983 ± 0.071	0.003 ± 0.001	0.005 ± 0.004	0.017 ± 0.008	0.050 ± 0.011

This is the peer-reviewed, final accepted version for American Mineralogist, published by the Mineralogical Society of America.
The published version is subject to change. Cite as Authors (Year) Title. American Mineralogist, in press.
DOI: https://doi.org/10.2138/am-2022-8241. http://www.minsocam.org/

Table 5. Representative oxygen isotopic compositions and Zr-in-titanite temperatures for titanite from the Notch Peak and Little Cottonwood stocks

Sample	Texture	^{18}O (‰ VSMOW	Temp (°C)
Notch Peak			
oNP-1-1-t4	1U	6.0	709
oNP-1-3b	1U	6.7	711
oNP-1-1-t5	1O	6.0	706
oNP-1-1l	2T	5.7	730
oNP-1-1m	2T	6.2	682
Notch Peak Aplite			
oNP-18-3a-1e	2F	6.1	714
Little Cottonwood			
oLC-HFT-1c	1O	4.7	707
oLC-HFT-7e	1S	5.4	710
oLC-SB-5c	1Pc	5.3	736
oLC-SB-1a	1Pc	4.6	760
oLC-HFT-8f	2A	4.6	630
oLC-HFT-7i	2B	2.6	-
Little Cottonwood mafic enclaves			
oLC-HFT-18-6-5d	1U	5.3	708
oLC-SB-18-5-2e	1U	4.8	703
oLC-HFT-18-6-1c	1U	5.6	724
oLC-SB-18-5-5c	1Pc	5.2	714
oLC-HFT-18-6-3g	2A	5.3	678

This is the peer-reviewed, final accepted version for American Mineralogist, published by the Mineralogical Society of America.
The published version is subject to change. Cite as Authors (Year) Title. American Mineralogist, in press.
DOI: https://doi.org/10.2138/am-2022-8241. http://www.minsocam.org/

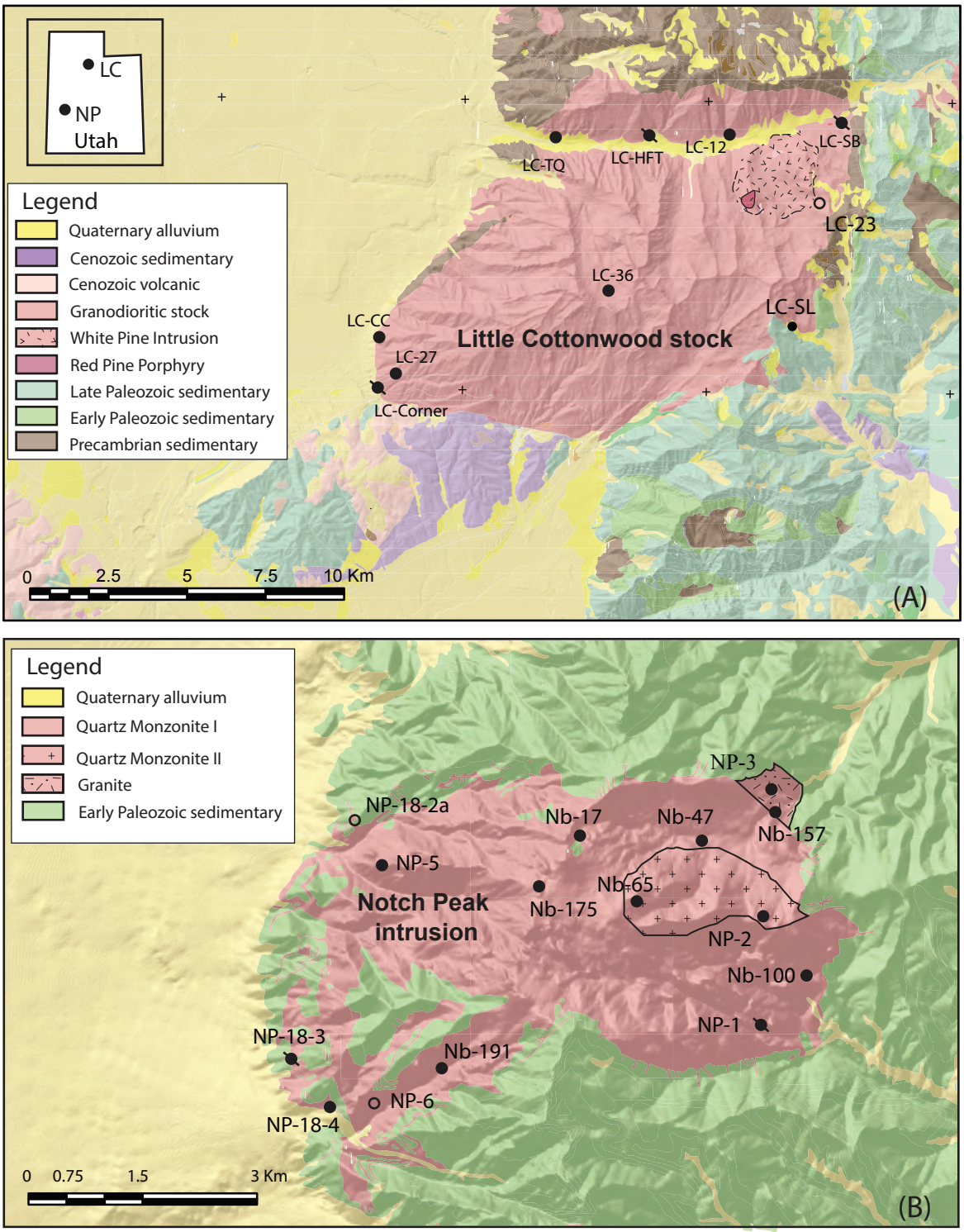

Figure 1. Geologic maps of the (A) Little Cottonwood and (B) Notch Peak plutons, Utah, with sample locations. Altered samples are represented by un¬filled circles. Samples in which Ttn was analyzed for its oxygen isotopic composition are marked with diagonal slashes. Map for the Little Cottonwood area is modified from Constenius et al. (2011) and Jensen (2019); the Notch Peak map is modified from Hintze and Davis (2002) and Nabelek et al (1983).

This is the peer-reviewed, final accepted version for American Mineralogist, published by the Mineralogical Society of America.
The published version is subject to change. Cite as Authors (Year) Title. American Mineralogist, in press.
DOI: https://doi.org/10.2138/am-2022-8241. http://www.minsocam.org/

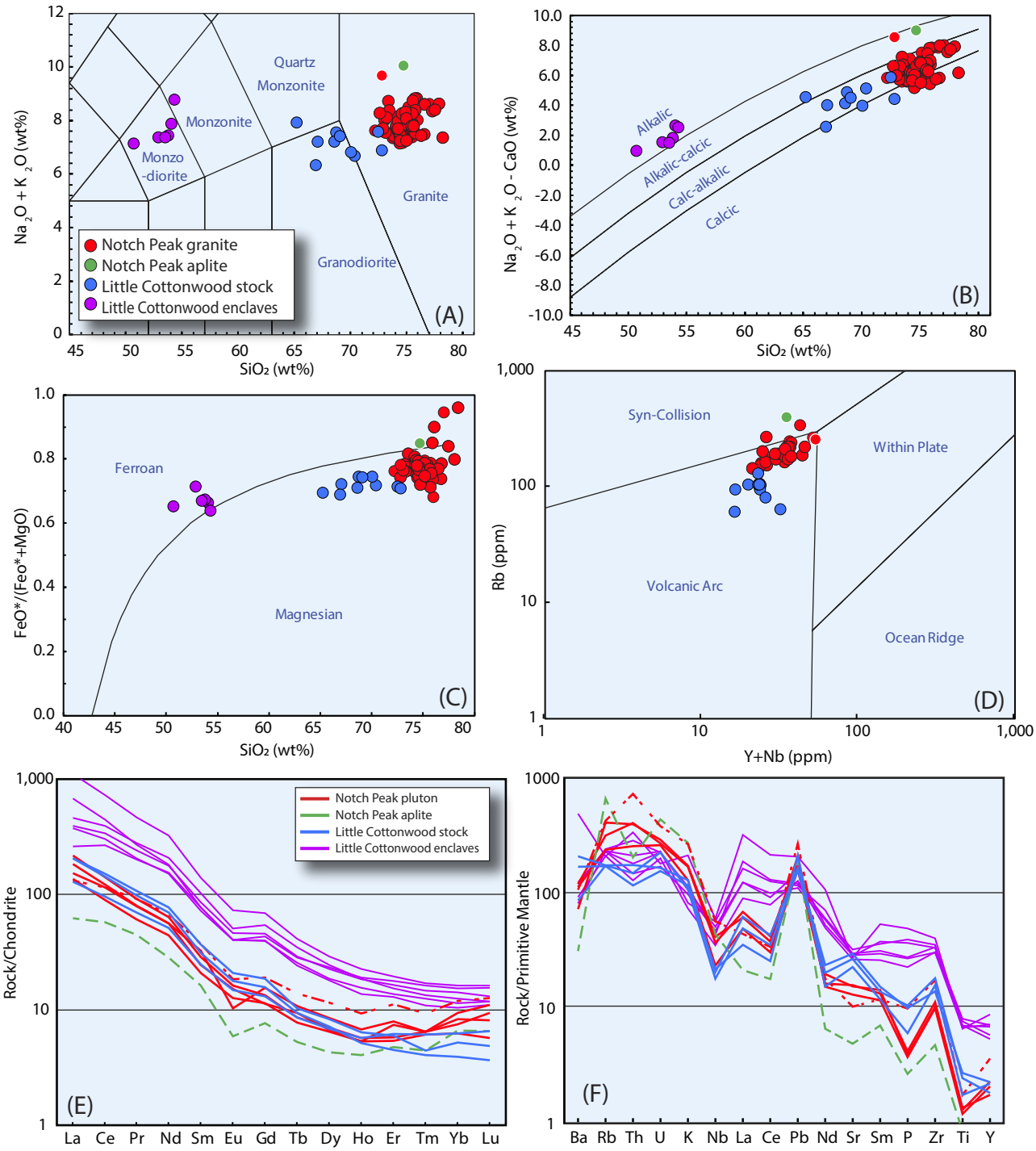

Figure 2. Whole-rock compositions of the plutonic rocks. (A) Total alkali-silica diagram (Le Bas et al. 1986). (B) Modified alkali-lime index (Frost et al. 2001). (C) Low FeO/(FeO+MgO) ratios indicate the oxidized character of the magmas (Miyashiro 1974). (D) Trace element concentrations of are consistent with a subduction origin for the plutons (Pearce et al., 1984). (E) Chondrite-normalized REE patterns. Monzodioritic Little Cottonwood enclaves are much more enriched in REE than the granitic host rocks. (F) Mantle-normalized trace element patterns. Chondrite and primitive mantle values taken from McDonough and Sun (1995). Hydrothermally altered samples are designated with either a dashed line (E and F) or as open symbols.

This is the peer-reviewed, final accepted version for American Mineralogist, published by the Mineralogical Society of America.
The published version is subject to change. Cite as Authors (Year) Title. American Mineralogist, in press.
DOI: https://doi.org/10.2138/am-2022-8241. http://www.minsocam.org/

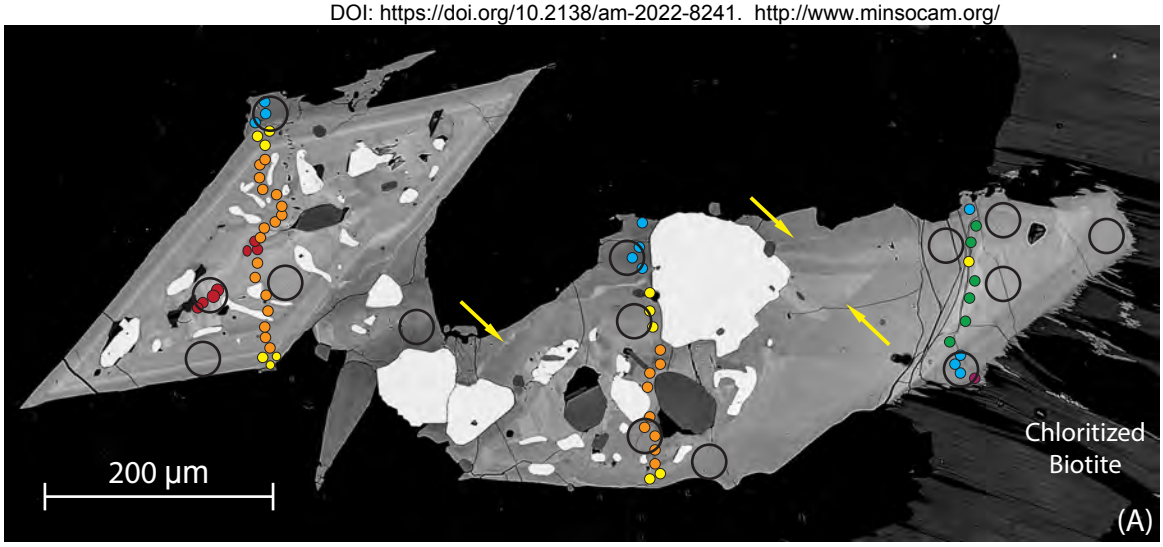

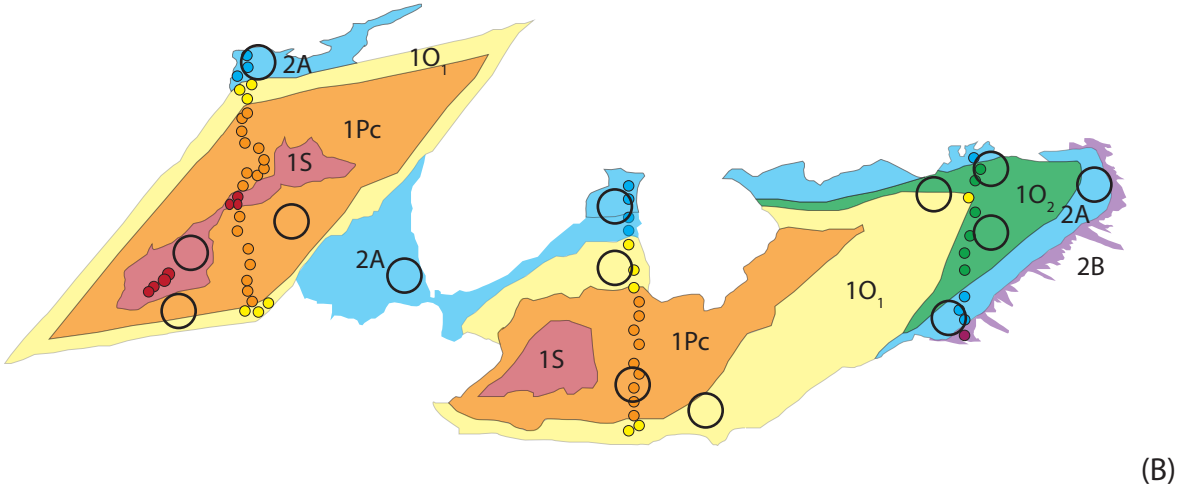

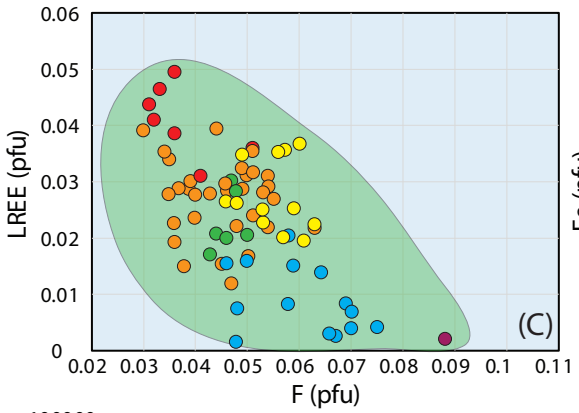

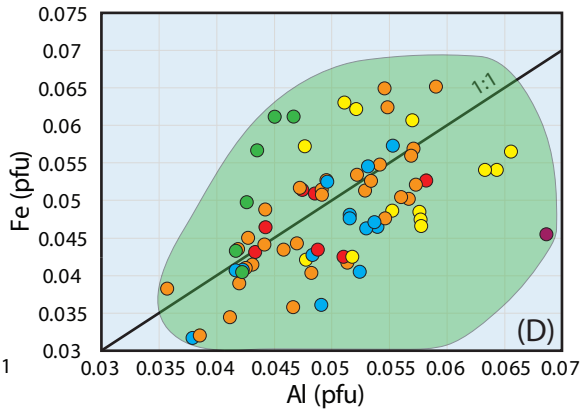

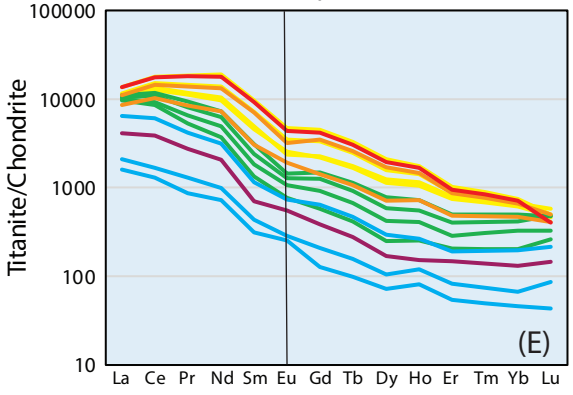

Figure 3. Titanite compositions correlate with the textural types as shown by this grain (LC-SB-4) from the Little Cottonwood stock. (A) BSE image with color coded spots for EMP and black circles for LA-ICP-MS analyses. Yellow arrows point to some dissolution surfaces. (B) Textural map of the grain showing several periods of magmatic and post-magmatic growth. (C) F concentrations increase and REE concentrations decrease from core to rim, especially in secondary Ttn (2A and 2B). The green field shows the range of all data from the Little Cottonwood stock. (D) Fe and Al concentrations largely overlap for the different types. Titanite replacing Bt (type 2B), however, has low Fe/Al ratios. (E) REE concentrations are low in the outermost oscillatory zones (green 1O2) and in the secondary non-magmatic Ttn (cyan 2A and purple 2B). Secondary types also lack negative Eu anomalies.

This is the peer-reviewed, final accepted version for American Mineralogist, published by the Mineralogical Society of America.
The published version is subject to change. Cite as Authors (Year) Title. American Mineralogist, in press.
DOI: https://doi.org/10.2138/am-2022-8241. http://www.minsocam.org/

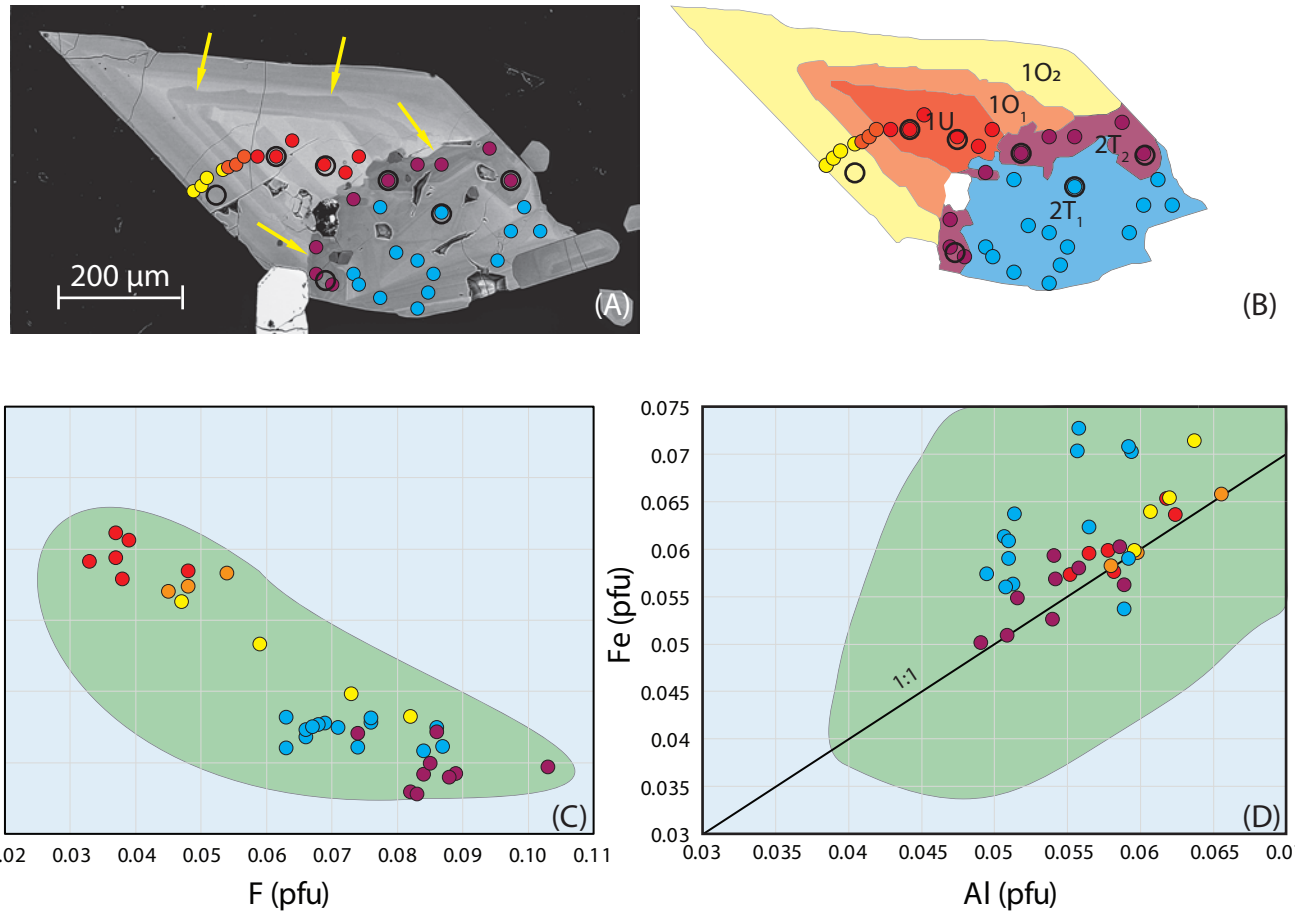

Figure 4. Titanite compositions and textural types for Notch Peak grain (NP-6-4). Colors represent di¬fferent zones. (A) BSE image and analytical spots—EMPA (colored coded by type of zoning) was followed by LA analysis (black circles). Yellow arrows point to dissolution surfaces. (B) Textural map of the grain reveals two periods of oscillatory growth (1O1 and 1O2) and two types of secondary hydrothermal Ttn (2T1 and 2T2). (C) F concentrations increase and REE concentrations decrease from core to rim and are especially low in the secondary zones (2T blue and purple). The green fields include all the data from the Notch Peak granite. (D) Fe and Al concentrations overlap for the di¬fferent types, but Fe/Al ratios are higher in the secondary hydrothermal Ttn (cyan and purple) and Al extends to lower values for the secondary types. (E) REE patterns. Yellow, orange, and red zones are primary magmatic Ttn and have high REE concentrations, lower La/Yb ratios, middle REE enrichment and negative Eu anomalies. The hydrothermal Ttn lacks the middle REE enrichment of typical magmatic Ttn and lacks negative Eu anomalies in 3 of the 4 analyses.

This is the peer-reviewed, final accepted version for American Mineralogist, published by the Mineralogical Society of America.
The published version is subject to change. Cite as Authors (Year) Title. American Mineralogist, in press.
DOI: https://doi.org/10.2138/am-2022-8241. http://www.minsocam.org/

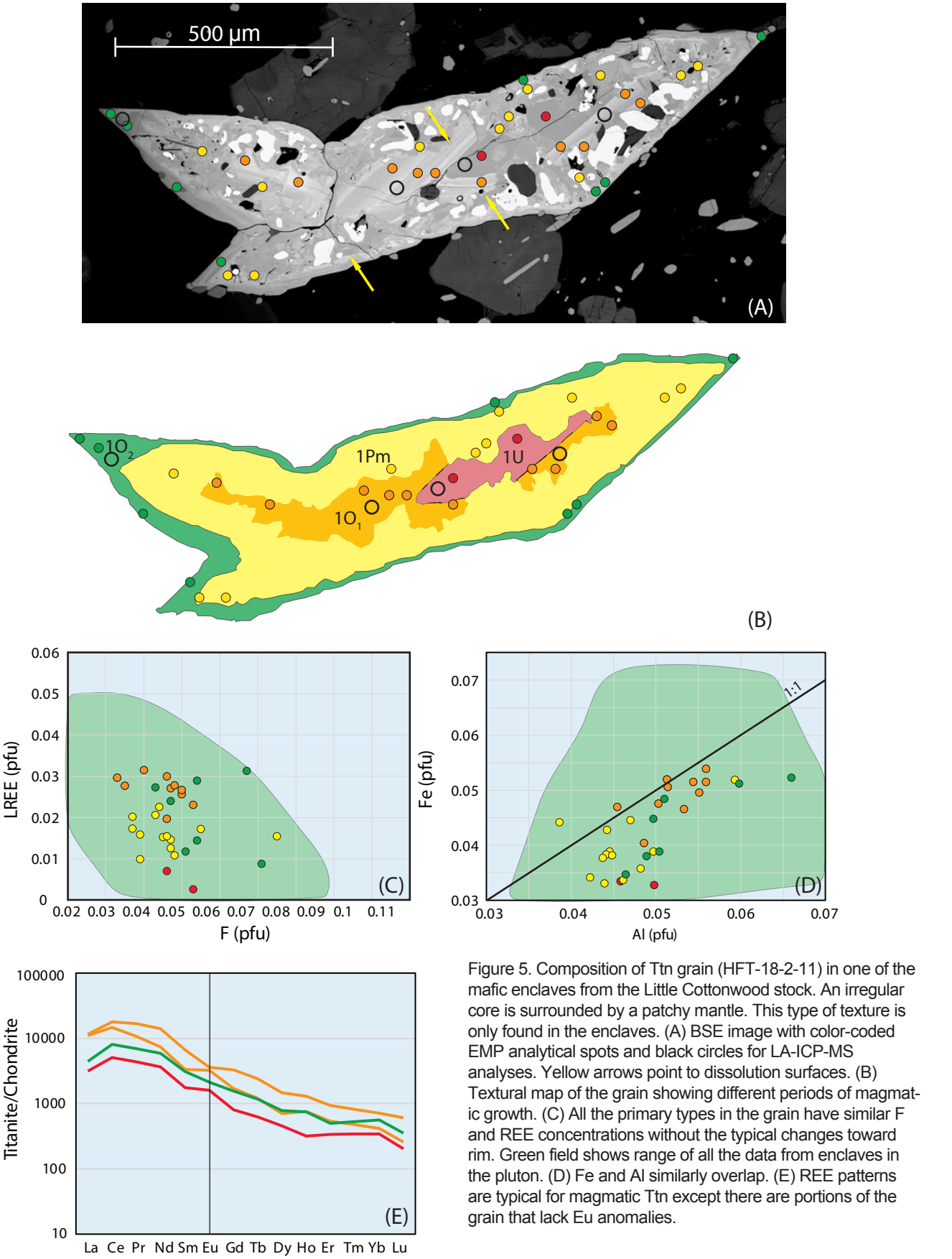

Figure 5. Composition of Ttn grain (HFT-18-2-11) in one of the mafic enclaves from the Little Cottonwood stock. An irregular core is surrounded by a patchy mantle. This type of texture is only found in the enclaves. (A) BSE image with color-coded EMP analytical spots and black circles for LA-ICP-MS analyses. Yellow arrows point to dissolution surfaces. (B) Textural map of the grain showing different periods of magmatic growth. (C) All the primary types in the grain have similar F and REE concentrations without the typical changes toward rim. Green field shows range of all the data from enclaves in the pluton. (D) Fe and Al similarly overlap. (E) REE patterns are typical for magmatic Ttn except there are portions of the grain that lack Eu anomalies.

This is the peer-reviewed, final accepted version for American Mineralogist, published by the Mineralogical Society of America.
The published version is subject to change. Cite as Authors (Year) Title. American Mineralogist, in press.
DOI: https://doi.org/10.2138/am-2022-8241. http://www.minsocam.org/

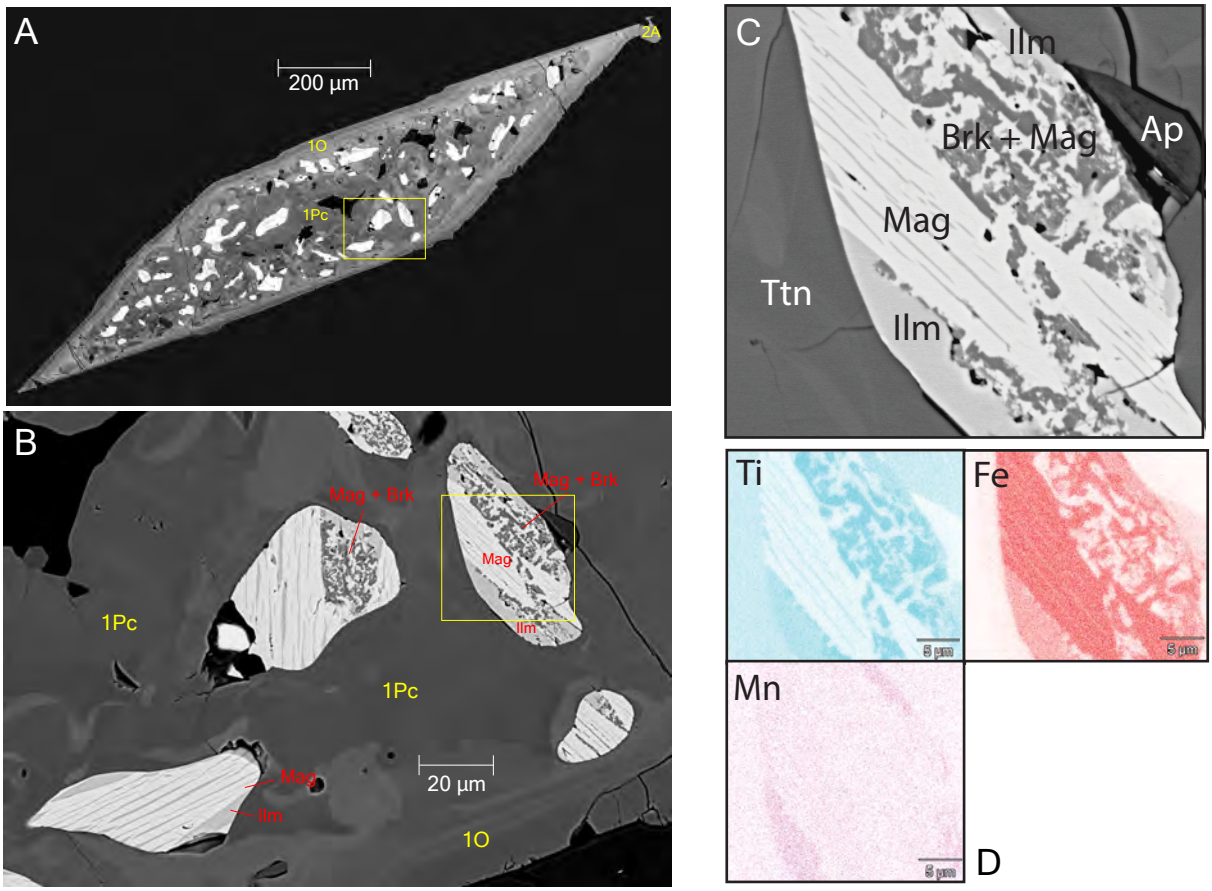

Figure 6. Patchy cores (1Pc) in Ttn are made of alternating dark and bright zones with highly irregular shapes, gradational to sharp wavy boundaries, and resorbed inclusions of Ilm (A) as seen here in grain LC-HFT-1. The greater magnification in (B) shows the details of this mottled texture. The Ilm inclusions have experienced subsolidus oxy-exsolution and now consist of Ilm (Ilm), brookite (Brk), and Mag (Mag). These patchy cores are prominent in Ttn from the Little Cottonwood stock but are uncommon or absent in Notch Peak granite. (C) BSE image of area in yellow box in B. (D) Maps of Ti, Fe, and Mn for grain in C. Magmatic high-Fe Ilm inclusions experienced oxy-exsolution to form Ilm (Ilm - pink on the Mn map and light gray on BSE image), low-Ti Mag (Mag - dark red on the Fe map and white on BSE image), and brookite (Brk, dark blue in Ti and white on Fe maps and dark gray on BSE image) in the slowly cooled plutons.

This is the peer-reviewed, final accepted version for American Mineralogist, published by the Mineralogical Society of America.
The published version is subject to change. Cite as Authors (Year) Title. American Mineralogist, in press.
DOI: https://doi.org/10.2138/am-2022-8241. http://www.minsocam.org/

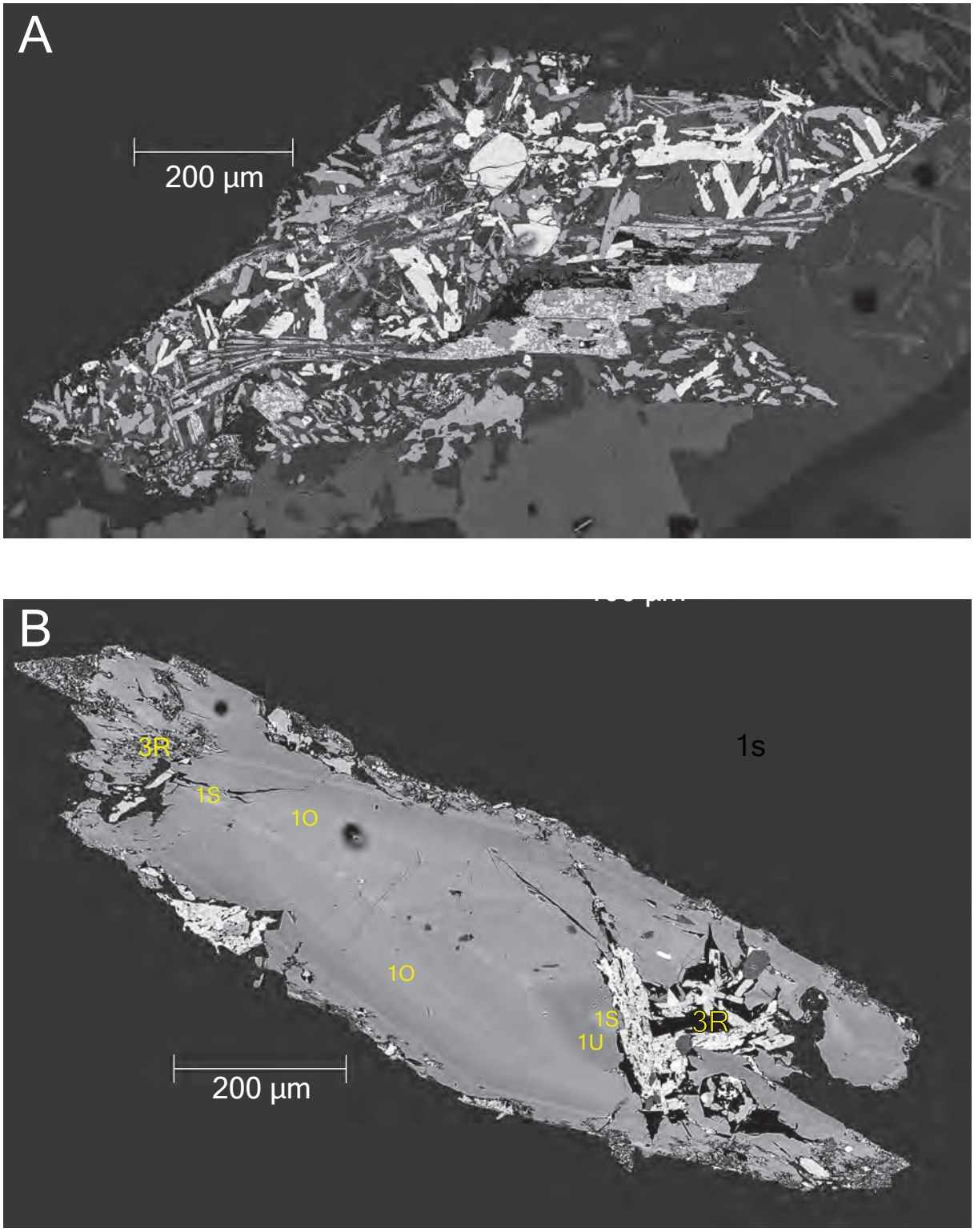

Figure 7. Replacement of Ttn (3R) in the Notch Peak pluton. (A) Grain NP-005-6 has been completely replaced by secondary Ilm, brookite, Mag, Bt, monazite, xenotime, Nb-Ti oxides, Ca-REE-fluorides, and Qz, but retains the original shape of the crystal. (B) Grain NP-002-5 has only some areas replaced. Unzoned (1U), oscillatory (1O), and bright sectors (1S) are also present.

This is the peer-reviewed, final accepted version for American Mineralogist, published by the Mineralogical Society of America.
The published version is subject to change. Cite as Authors (Year) Title. American Mineralogist, in press.
DOI: https://doi.org/10.2138/am-2022-8241. http://www.minsocam.org/

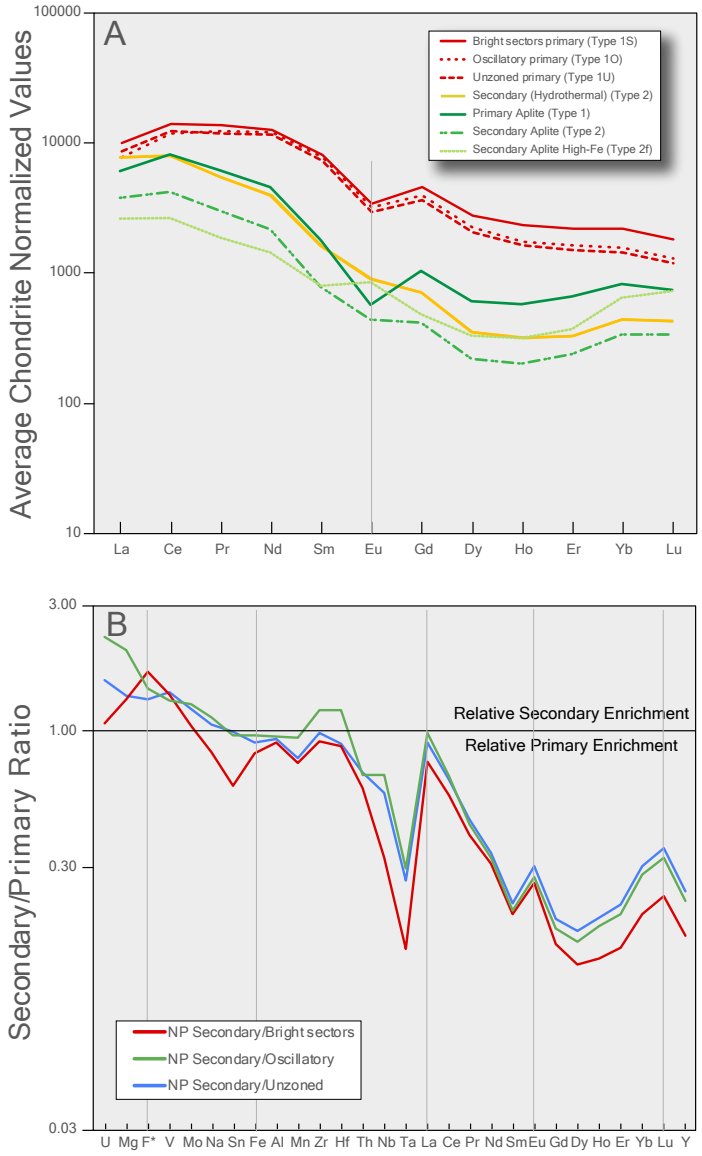

Figure 8. Composition of Ttn from the Notch Peak pluton. A) REE patterns of different Ttn zones reveal the depletion of REE in secondary hydrothermal Ttn (all types of secondary combined). B) The composition of average hydrothermal Ttn divided by average magmatic Ttn (LA-ICPMS data except for F, Fe, and Al which are from EMPA).

This is the peer-reviewed, final accepted version for American Mineralogist, published by the Mineralogical Society of America.
The published version is subject to change. Cite as Authors (Year) Title. American Mineralogist, in press.
DOI: https://doi.org/10.2138/am-2022-8241. http://www.minsocam.org/

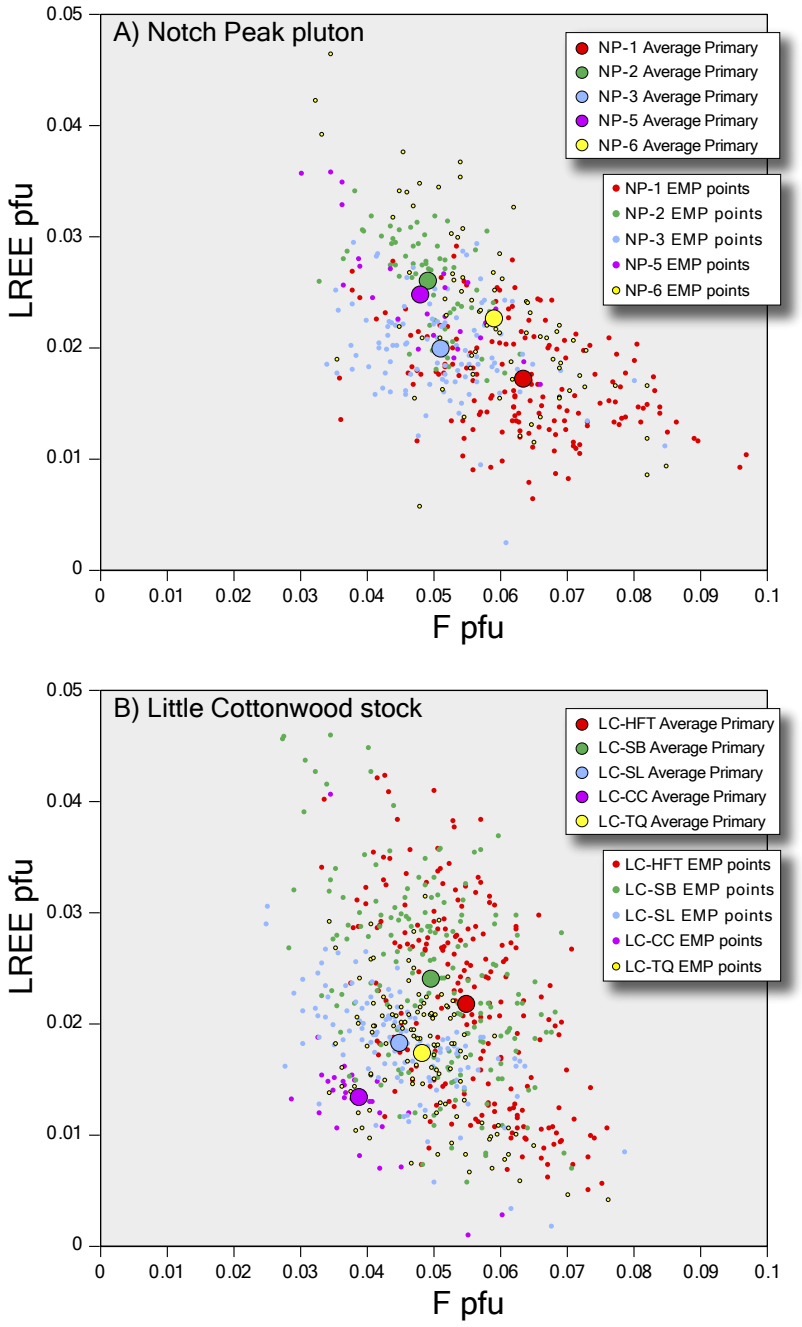

Figure 9. F versus LREE (by EMPA) in (A) Little Cottonwood stock and (B) Notch Peak pluton. According to t-tests, the means are significantly different with the exception of LC-SL and LC-TQ and NP-2 and NP-5.

This is the peer-reviewed, final accepted version for American Mineralogist, published by the Mineralogical Society of America.
The published version is subject to change. Cite as Authors (Year) Title. American Mineralogist, in press.
DOI: https://doi.org/10.2138/am-2022-8241. http://www.minsocam.org/

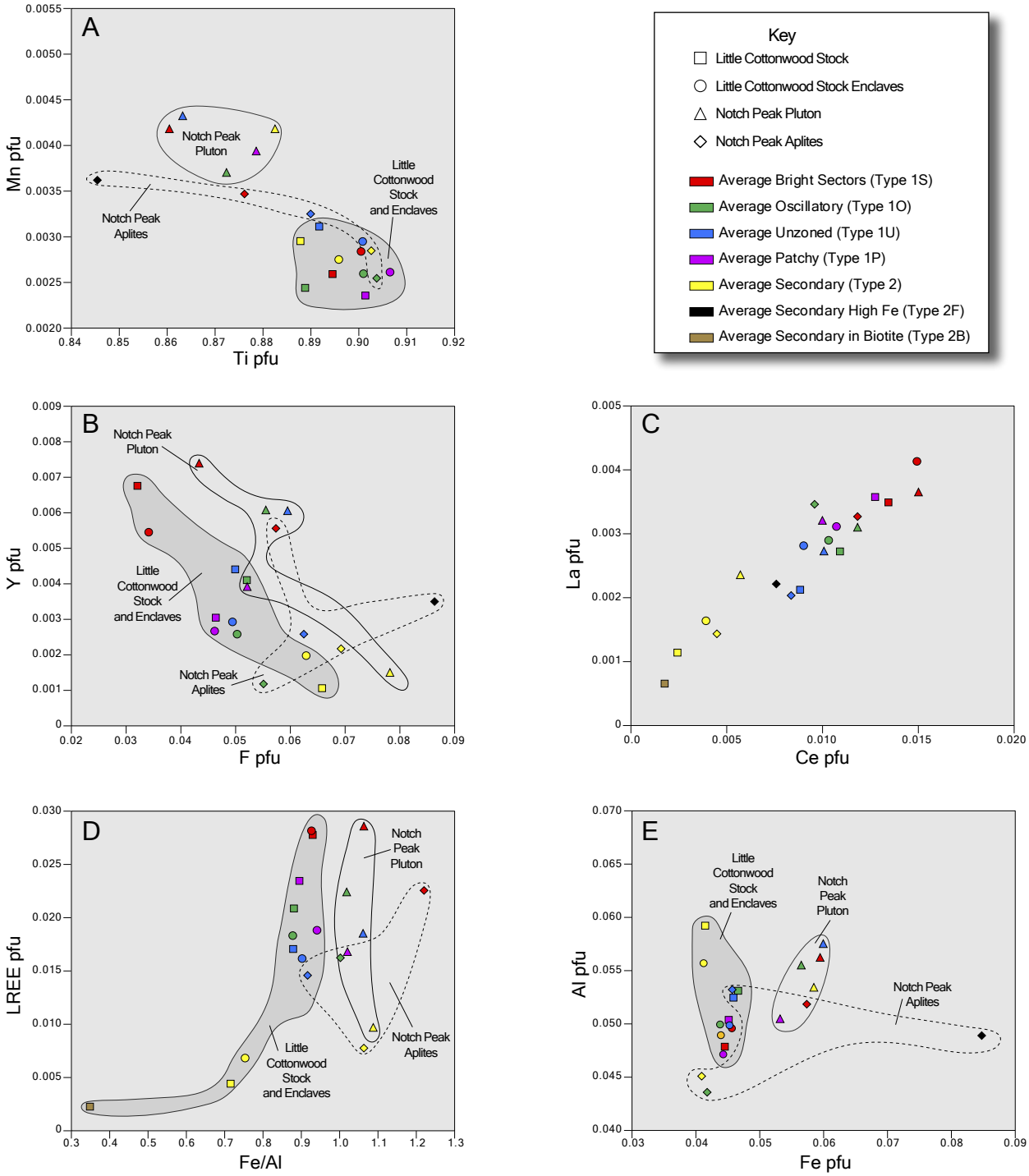

Figure 10. Average compositions (by EMPA) of Ttn in the different units studied. (A) Mn vs. Ti, (B) Y vs. F, (C) La vs. Ce, (D) LREE vs. Fe/Al ratio, and (E) Al vs Fe. On (D), the high-Fe Ttn type (2F) from the aplites is not plotted because the Fe/Al ratio is twice as high (>2.0) as other Notch Peak types. Likewise, type 2B (formed by Bt replacement) is not plotted on (A), (B), and (E) because of its high F and Al and low Ti concentrations. Typical secondary Ttn in the Little Cottonwood stock averages 0.07 F pfu, while type 2B averages 0.19 F pfu. Ti concentrations are low in type 2B (~0.75 pfu) because of very high Al (~0.20 pfu).

This is the peer-reviewed, final accepted version for American Mineralogist, published by the Mineralogical Society of America.
The published version is subject to change. Cite as Authors (Year) Title. American Mineralogist, in press.
DOI: https://doi.org/10.2138/am-2022-8241. http://www.minsocam.org/

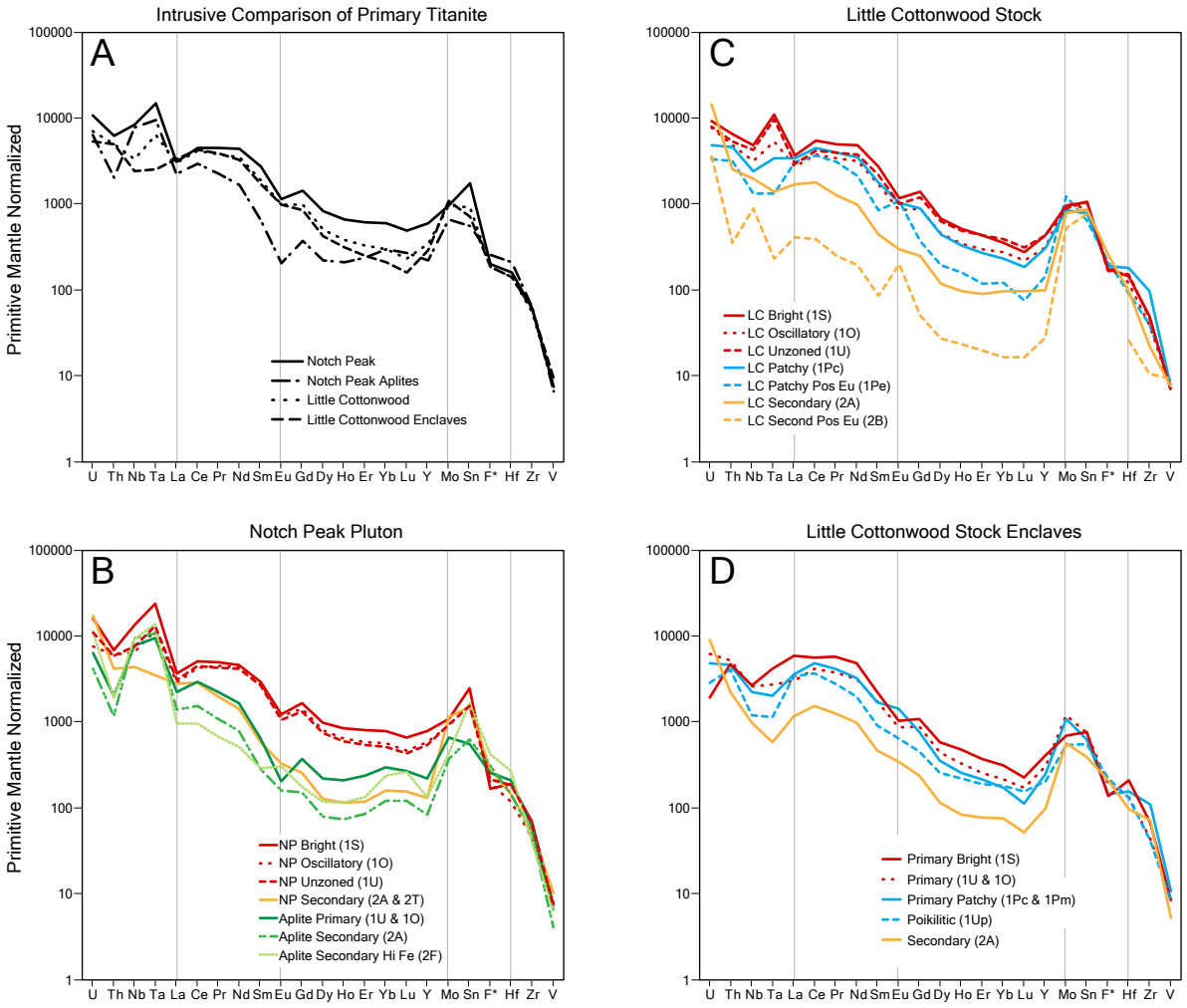

Figure 11. Primitive mantle normalized plots of average Ttn compositions (LA-ICP-MS analyses except for F by EMPA). (A) Primary Ttn from Notch Peak has higher concentrations of most plotted elements than their counterparts from Little Cottonwood stock, but Ttn from Notch Peak aplites has distinctly lower concentrations of REE. Comparison of primary and secondary Ttn: (B) Notch Peak; (C) Little Cottonwood stock; and (D) Little Cottonwood enclaves (D). Compared to primary Ttn, secondary Ttn is generally depleted in all these elements, except U and F.

This is the peer-reviewed, final accepted version for American Mineralogist, published by the Mineralogical Society of America.
The published version is subject to change. Cite as Authors (Year) Title. American Mineralogist, in press.
DOI: https://doi.org/10.2138/am-2022-8241. http://www.minsocam.org/

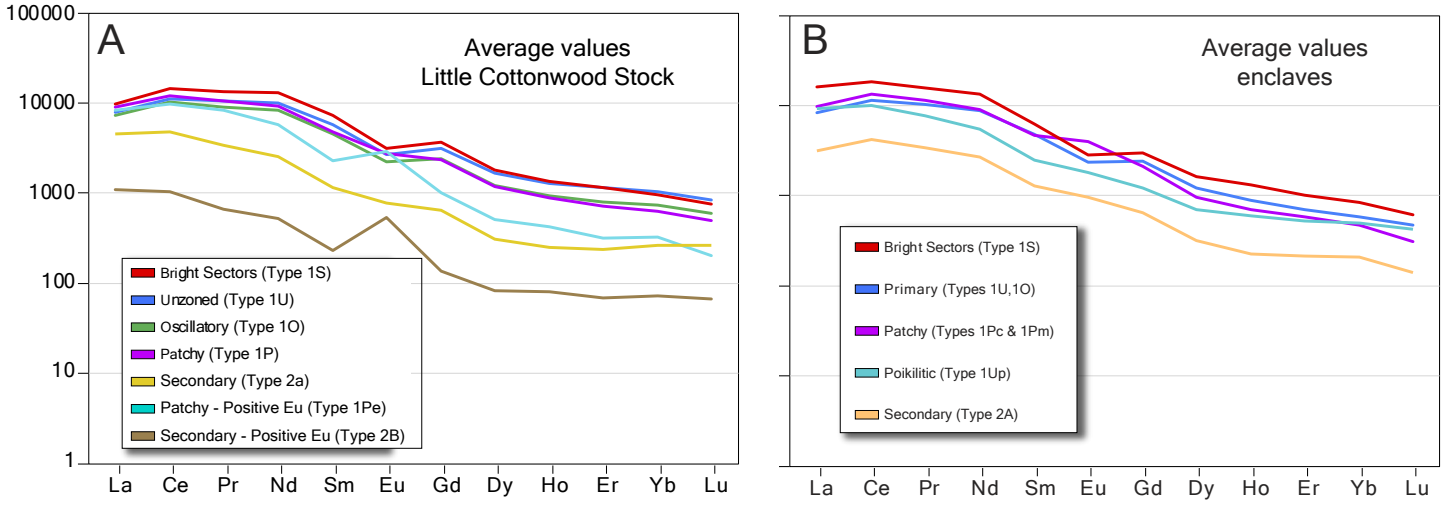

Figure 12. Chondrite-normalized REE plots for different types of titanite in the Little Cottonwood stock. (A) REE patterns for titanite in granodiorite. Bright sectors (1S) unzoned (1U), oscillatory (1O), and patchy core (1Pc) types have similar REE patterns, although the patchy cores tend to have smaller Eu anomalies. Secondary titanite grains have lower REE contents and lack Eu anomalies, except for type 2B which has strong positive Eu anomalies. Some analyses of patchy zones also have strong positive Eu anomalies (1Pe) that and may be evidence for a secondary origin. (B) REE patterns for titanite from enclaves in the Little Cottonwood stock. Plots for individual analyses are in Supplement B.

This is the peer-reviewed, final accepted version for American Mineralogist, published by the Mineralogical Society of America.
The published version is subject to change. Cite as Authors (Year) Title. American Mineralogist, in press.
DOI: https://doi.org/10.2138/am-2022-8241. http://www.minsocam.org/

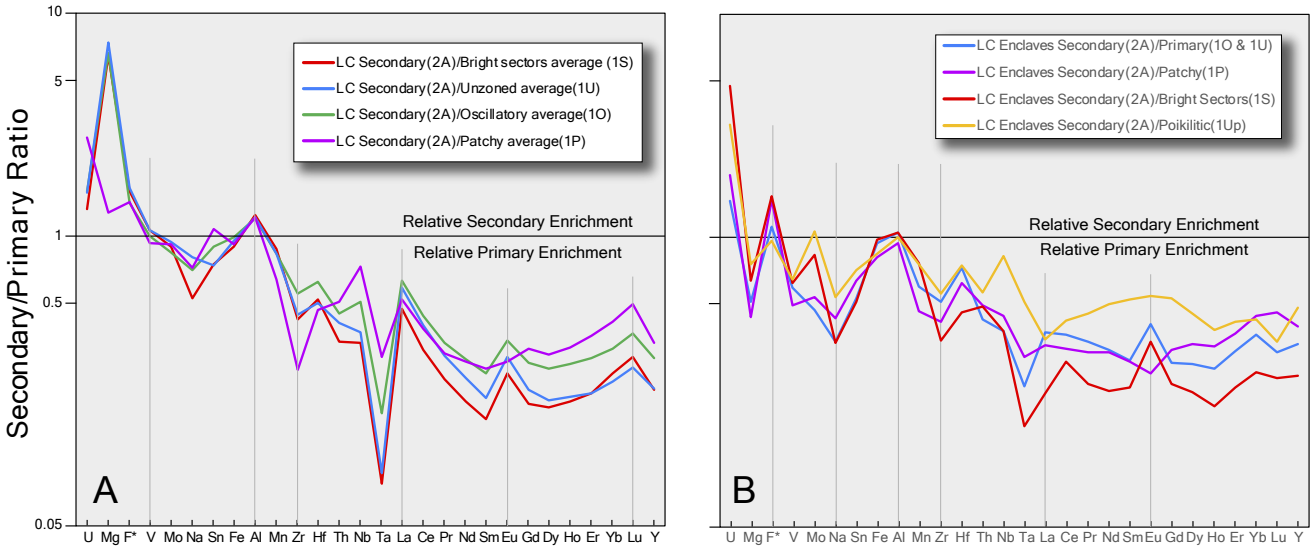

Figure 13. Comparisons of magmatic and hydrothermal titanite in the Little Cottonwood stock. (A) Ratio of composition of average secondary to primary titanite in granodiorite. Secondary titanite (2A) is enriched in U, Mg, F, and Al and has low middle REE (Nd to Er), and anomalous Eu compared to primary titanite. (B) Ratio of the composition of average secondary titanite to primary titanite in the mafic enclaves. Secondary titanite (2A) is enriched in U and F and has anomalous Eu compared to primary titanite.

This is the peer-reviewed, final accepted version for American Mineralogist, published by the Mineralogical Society of America.
The published version is subject to change. Cite as Authors (Year) Title. American Mineralogist, in press.
DOI: https://doi.org/10.2138/am-2022-8241. http://www.minsocam.org/

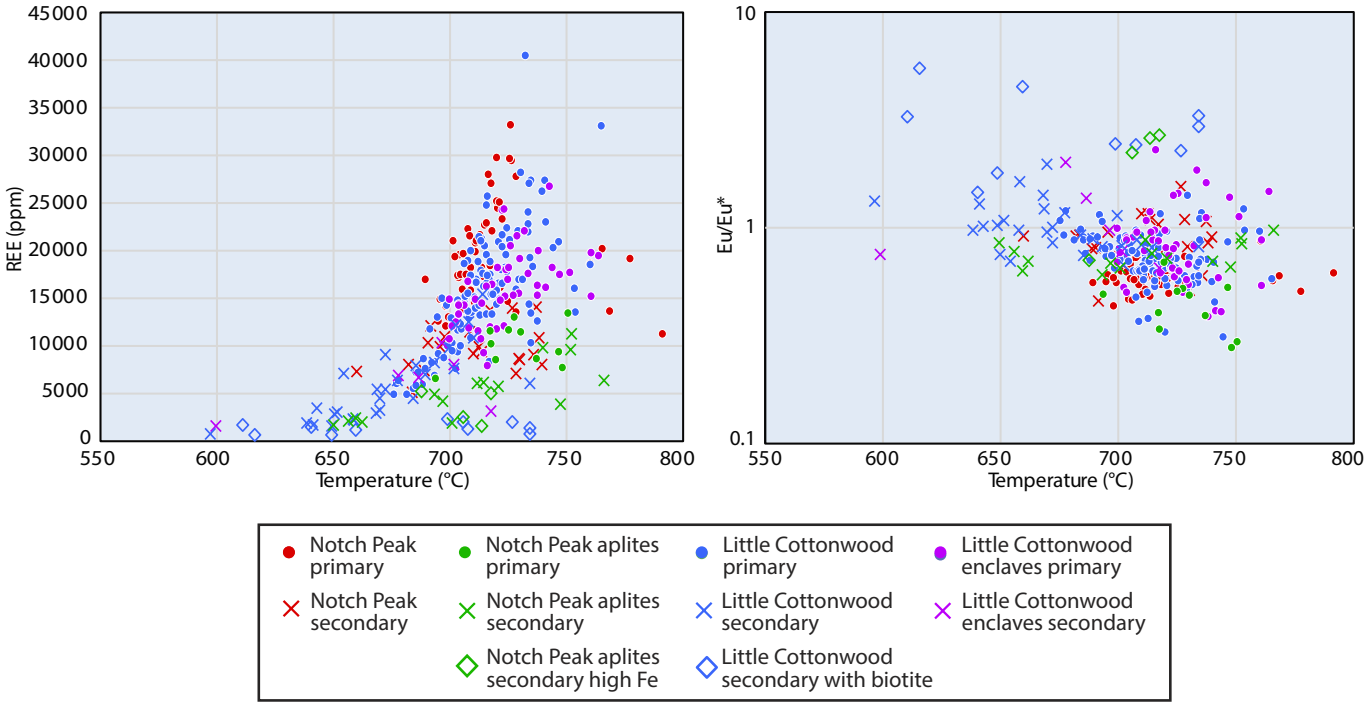

Figure 14. Zr-in-Ttn temperatures. Temperature vs. (A) total REE and (B) Eu/Eu*. Compared to primary magmatic Ttn (circles), secondary Ttn (x) in the Little Cottonwood stock tends to yield lower calculated T (700°C) and positive Eu anomalies (Eu/Eu* >1). Eu was not as mobile during precipitation of secondary Ttn in the Notch Peak intrusion based on the overlap of Eu/Eu* for the two types. In the Little Cottonwood stock, secondary Ttn associated or intergrown with Bt (type 2B) has the highest Eu/Eu*, while at Notch Peak the high Fe zones in Ttn from the aplites have the highest Eu/Eu*. Zr-in-Ttn temperatures were calculated using 0.75 as the $a\mathrm{TiO_2}$.

This is the peer-reviewed, final accepted version for American Mineralogist, published by the Mineralogical Society of America.
The published version is subject to change. Cite as Authors (Year) Title. American Mineralogist, in press.
DOI: https://doi.org/10.2138/am-2022-8241. http://www.minsocam.org/

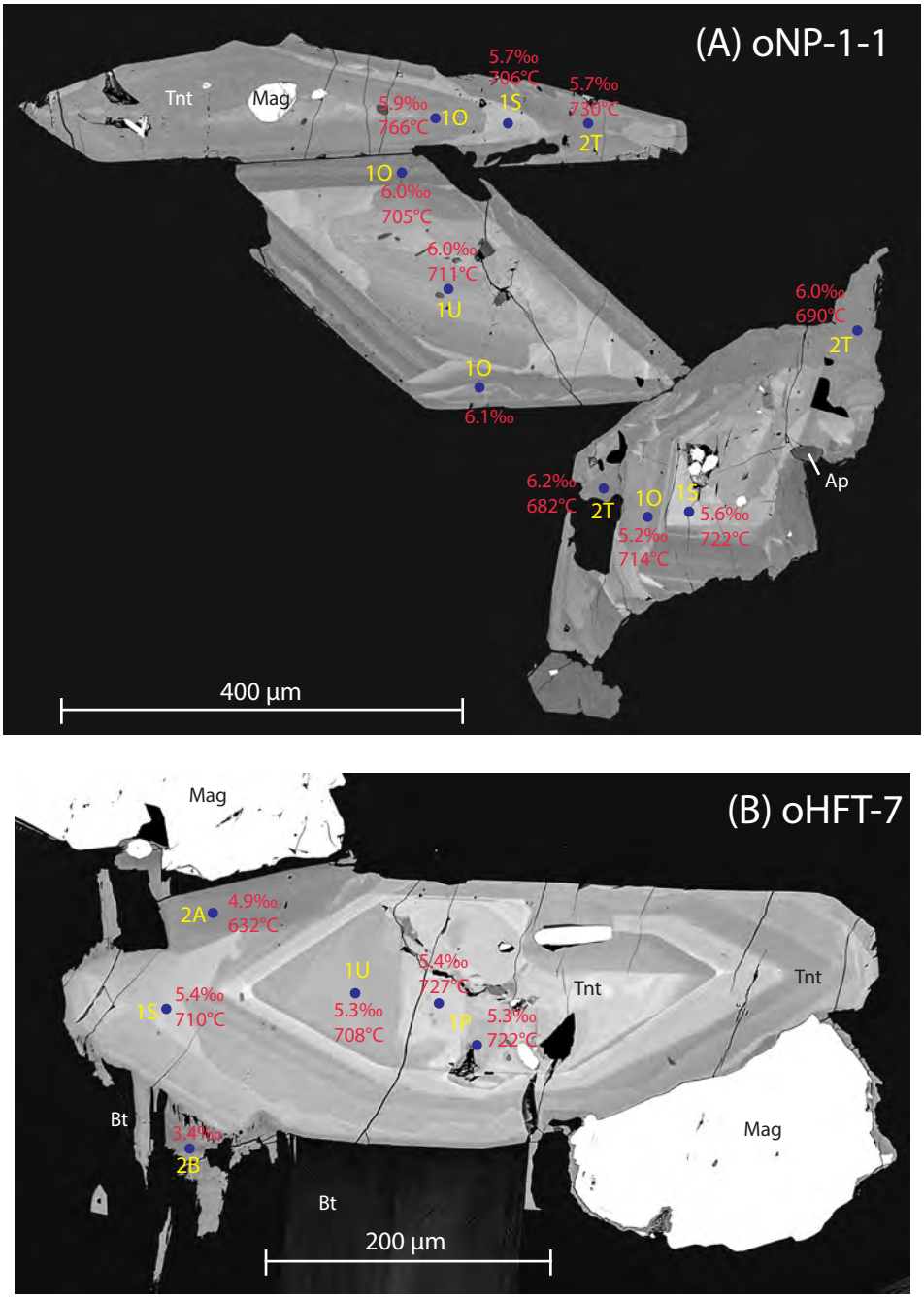

Figure 15. Spot maps of two grains (oNP-1 and oHFT-7) showing $\delta^{18}O$ and Zr-in-Ttn temperatures (except for the 2B zone on HFT-7 that was too small to analyze by LA-ICP-MS). Primary (1S,1U, and 1O) and secondary types (2A) have similar $\delta^{18}O$ values, with 2A slightly lower. Titanite associated with Bt (2B) is lower still (2.3‰) suggesting interaction with meteoric water with low $\delta^{18}O$.

This is the peer-reviewed, final accepted version for American Mineralogist, published by the Mineralogical Society of America.
The published version is subject to change. Cite as Authors (Year) Title. American Mineralogist, in press.
DOI: https://doi.org/10.2138/am-2022-8241. http://www.minsocam.org/

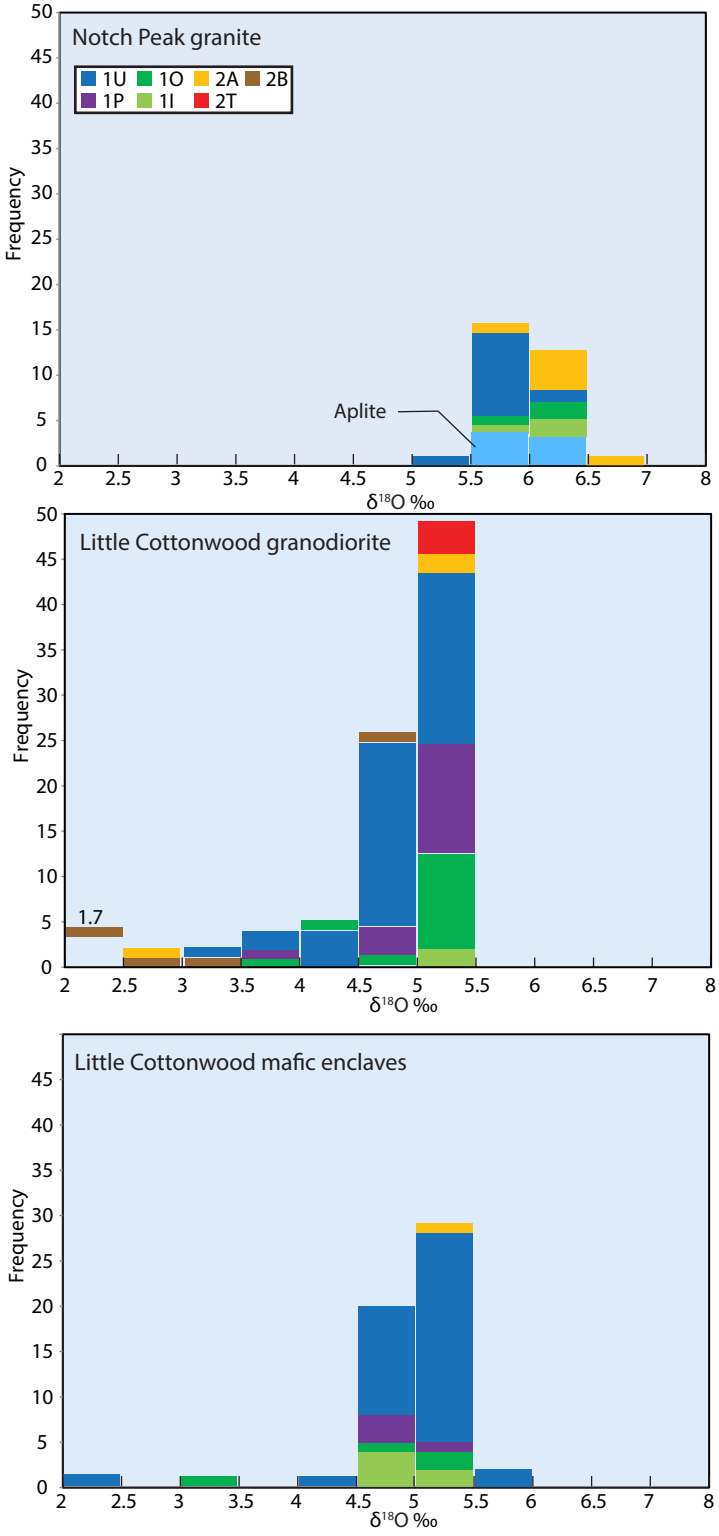

Figure 16. Histograms of δ18O values in titanite collected using SIMS. δ18O values for primary titanite from the Notch Peak pluton are typically higher than for titanite from the Little Cottonwood stock (6.0‰ vs. 4.9‰), reflecting the original magmatic compositions. δ18O of secondary titanite (2A) in the Notch Peak pluton extends to slightly higher values than for primary titanite, while secondary titanite in the Little Cottonwood stocks tends to have lower δ18O, especially in titanite replacing biotite (2B).

This is the peer-reviewed, final accepted version for American Mineralogist, published by the Mineralogical Society of America.
The published version is subject to change. Cite as Authors (Year) Title. American Mineralogist, in press.
DOI: https://doi.org/10.2138/am-2022-8241. http://www.minsocam.org/

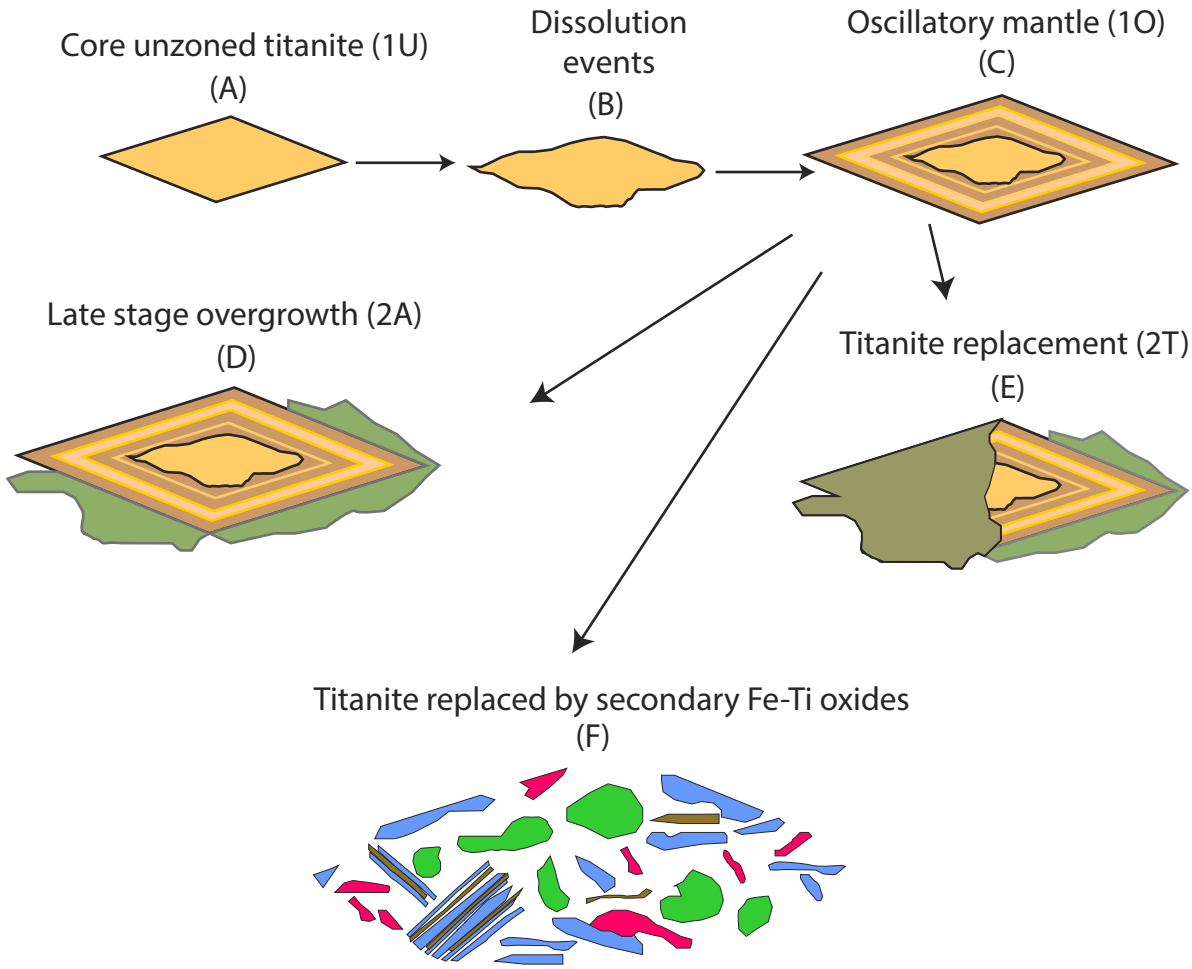

Figure 17. Crystallization of Ttn in the Notch Peak granite. (A) Unzoned Ttn (1U) crystallized from granitic magma. (B) Sporadic dissolution events resorbed part of this grain. (C) New growth of magmatic Ttn mantled the unzoned core, usually with oscillations (1O) linked to sector zones (1S). (D) At a later stage, secondary Ttn (2A) crystallized from exsolved magmatic fluid to form BSE dark (REE-Y-poor, F-rich) anhedral overgrowths. (E) Some grains were partially replaced by BSE-dark secondary Ttn (2T). (F) Locally, Ttn was completely replaced by secondary minerals (3R), including Ilm (blue), Mag (green), Bt (brown) and a TiO_2 phase (red), during reaction with oxidized fluid.

This is the peer-reviewed, final accepted version for American Mineralogist, published by the Mineralogical Society of America.
The published version is subject to change. Cite as Authors (Year) Title. American Mineralogist, in press.
DOI: https://doi.org/10.2138/am-2022-8241. http://www.minsocam.org/

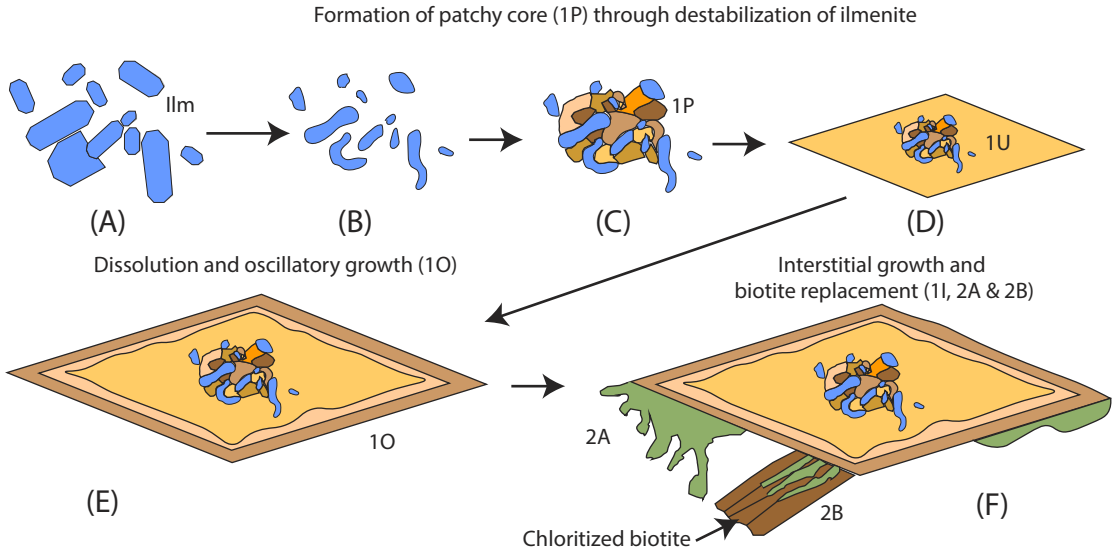

Figure 18. A typical crystallization path for Ttn in the Little Cottonwood stock. (A) Ilmenite (blue) grew in low fO_2, monzondioritic magma. (B) Ilmenite was resorbed when this magma mixed with higher fO_2 calc-alkaline felsic magma. (C) Patchy Ttn (1P) grew during the reaction of Ilm with the felsic magma and preserved partially resorbed Ilm. (D) After mixing, unzoned Ttn (1U) mantled the core. (E) Oscillatory growth (1O) ensued to form the rim of the grain. Growth and dissolution alternated. (F) Secondary Ttn formed as BSE-dark anhedral overgrowths (2A) or F-rich REE-poor blade-like anhedra (2B) where Bt reacted with fluid to stabilize Chl.